Studies on Dispersive Stabilization of Porous Media Flows

Prabir Daripa* and Craig Gin

Department of Mathematics, Texas A&M University, College Station, TX-77843

August 4, 2016

Abstract

Motivated by a need to improve the performance of chemical enhanced oil recovery (EOR) processes, we investigate dispersive effects on the linear stability of three-layer porous media flow models of EOR for two different types of interfaces: permeable and impermeable interfaces. Results presented are relevant for the design of smarter interfaces in the available parameter space of Capillary number, Peclet number, longitudinal and transverse dispersion and the viscous profile of the middle layer. The stabilization capacity of each of these two interfaces is explored numerically and conditions for complete dispersive stabilization are identified for each of these two types of interfaces. Key results obtained are: (i) three-layer porous media flows with permeable interfaces can be almost completely stabilized by diffusion if the optimal viscous profile is chosen; (ii) flows with impermeable interfaces can also be almost completely stabilized for short time, but become more unstable at later times because diffusion flattens out the basic viscous profile; (iii) diffusion stabilizes short waves more than long waves which leads to a "turning point" Peclet number at which short and long waves have the same growth rate; and (iv) mechanical dispersion further stabilizes flows with permeable interfaces but in some cases has a destabilizing effect for flows with impermeable interfaces, which is a surprising result. These results are then used to give a comparison of the two types of interfaces. It is found that for most values of the flow parameters, permeable interfaces suppress flow instability more than impermeable interfaces.

Keywords: Porous media flows, Linear stability, Diffusion, Mechanical dispersion, Eigenvalue problem

*Author for correspondence (e-mail: prabir.daripa@math.tamu.edu)

1 Introduction

Developments in the last five decades have made it clear that in displacement processes in which a viscous fluid such as water displaces a more viscous fluid such as oil, the mobility jump across an interface between two such fluids renders the interface unstable to hydro-dynamical perturbations. The ensuing fingering and side-branching instabilities are now generally viewed as some of the primary causes of early breakthrough resulting in poor displacement efficiency of secondary oil recovery. This creates the need for the stabilization of such displacement processes which can be achieved by reducing the growth rates of unstable waves. It is now a well established fact from basic stability results (see [16]) that this requires reducing the mobility contrast between the displaced fluid (oil) and the displacing fluid by increasing the viscosity of the displacing fluid. This is done using polymer in water and using the resulting aqueous phase (to be called polysolution henceforth) as a displacing fluid instead of water. Flooding the reservoir first using such a polysolution phase and then followed by water has become a traditionally accepted solution to the stabilization problem. This method of flooding, called "polymer flooding", is one of the chemical Enhanced Oil Recovery (EOR) Methods. Polymer flooding has been studied extensively in the laboratory, tested widely in the field, and mathematically modeled, analyzed and simulated (see [11, 19, 21]).

The literature on the practice of polymer flooding is vast. In general, polymer-flooding as discussed above has three layers (or regions) of these phases (oil, polysolution, and water) to begin with. The three layers are perpendicular to the mean flow direction with the extreme layer fluids having constant viscosity. A good prototype model of this polymer flooding process (see [4]), which is accessible to analysis to gain physical insight into various processes, has been the three-layer Hele-Shaw model (see [5]). The polymer concentration in the polysolution can have a profile, and the concentration profile commonly chosen for maximum stabilization is a monotonic one so that the instability of the system is shouldered equally, roughly speaking, between the three entities: two individually unstable interfaces and an unstable middle layer (see [8]). It is known from this work that this configuration is the optimal one in the sense that any other configuration would make the flow more unstable with the exception of some in which the flow is approximately equally unstable. However, in practice, any specific profile of polymer concentration injected with the displacing fluid is certainly difficult to maintain as it flows due to various factors including the unsteady nature of the flow, adsorption, and diffusion of polymer from the polysolution phase to the adjacent water phase displacing the middle layer of polysolution. Because of these reasons, even an originally injected profile of uniform concentration of polymer will develop some non-uniformity. This non-uniformity in concentration induces species (polymer) diffusion within the polysolution phase itself. Therefore, it is important to study the effect of species diffusion within the middle layer on the stability of the flow.

Recently, the effect of such diffusion within the polysolution phase on the flow instability has been studied (see [14], [15]) using linear stability analysis and assuming the phases are immiscible and interfaces are impermeable to polymer meaning no diffusion of polymer from the polysolution phase into the adjacent water phase. This is not unrealistic since in practice one can use an infinitesimally thin layer of spacer fluid of non-aqueous phase liquid (NAPL) between these two phases. Alternatively, one can use simply an NAPL phase instead of the water phase to displace the polysolution phase (see Figure 2). Linear stability analysis of this flow model leads to an eigenvalue problem (see [14]), the analysis of which using classical techniques of partial differential equations provides an upper bound on the growth rate. To make the analysis possible, one of the boundary conditions in the eigenvalue problem is somewhat compromised in [14]. The upper

bound result there provides an indication that diffusion is stabilizing but not with complete conviction due to some inherent shortcomings in the argument (see [14]) used there. Because that study on the effect of diffusion on the stability of porous media flows is not conclusive enough and does not include (mechanical) dispersive effects that could potentially affect the stability of porous media flows as well, we undertake a complete and detailed study of the diffusive and (mechanical) dispersive effects in this work. **For purposes below, dispersion means the combined effect of diffusion and mechanical dispersion, unless mentioned otherwise to mean only mechanical dispersion.**

The effect of dispersion on the linear stability of Hele-Shaw and porous media flows has been studied for the cases of single-fluid flow and **miscible** flow [18, 20, 24, 25, 27, 32, 34]. However, to the best of the authors' knowledge, there has not been much study of mechanical dispersion for immiscible Hele-Shaw and porous media flows. Dispersion acts within the middle, variable-concentration layer. Since dispersion has been found to have an effect on stability for a single phase flow [32], it can have an effect on the stability of immiscible flow which we explore in this paper.

Throughout the previous studies on dispersion in porous media and Hele-Shaw flows, several different velocity-dependent models of dispersion have been used. In an early study of miscible flow, Tan and Homsy [27] used a model for dispersion that was derived by Perkins and Johnston [23] for a packed bed of particles. They found that for a step concentration profile, very large longitudinal dispersion (in comparison to transverse dispersion) increases the growth rate while very large transverse dispersion decreases the growth rate. A different model, which comes from adapting the seminal works of Taylor [29, 30] and Aris [1], was used by Wooding [32], Homsy and Zimmerman [34], Petitjeans et. al. [24], and Maes et. al. [20]. This Taylor-Aris model only has dispersion in the longitudinal direction and it depends quadratically on velocity. However, Petitjeans et. al. [24] found that the Taylor-Aris model does not match experimental data for certain parameter ranges. This is due to the fact that the Taylor-Aris model is based on an assumption of Poiseuille flow, which is a bad assumption for flows with large viscous gradients. Due to this fact, several investigators have used a model for dispersion in porous media flow set forth by Bear [2]. This model has been used in stability studies of miscible flows by Yortsos and Zeybek [33], Riaz et. al. [25], and Ghesmat and Azaiez [18]. This model is also popular in recent (non-stability) works on dispersion in porous media [17]. Therefore, we employ this model here (see section 5).

Thus we undertake a detailed linear stability study numerically to investigate the effects of diffusion and mechanical dispersion on the stability of the three-layer porous media flow model of EOR for two types of interfaces, namely impermeable and permeable. In particular, through this study we are looking for answers to some questions of fundamental physics which also have a bearing on chemical EOR. Some of these are as follows. Are diffusion and/or mechanical dispersion stabilizing in the available parameter space? Can mild diffusion and/or mechanical dispersion have a large stabilization effect? How does diffusion and/or dispersion individually affect an otherwise optimal viscous profile? Is complete stabilization possible by diffusion and/or dispersion? We address these and many other relevant stability issues for each of the two types of interfaces in an effort to also find which one of these two interfaces is more desirable and when. Answers to these and many other important stability related questions are answered in section 7 on conclusions which are supported by numerical evidence presented in sections 4 and 5.

This paper is laid out as follows. In section 2, we first recall the the mathematical model which incorporates diffusion only, followed by linear stability analysis when the interfaces are impermeable (section 2.1) as well as when the interfaces are permeable (section 2.2). The associated eigenvalue problems for both of these

case are summarized there. In section 3, we reformulate the eigenvalue problems in two variables into 4th order eigenvalue problems which are convenient for numerical computation. The numerical method to solve these eigenvalue problems is briefly described in Appendix-B. In section 4, numerical results are presented, discussed and critically analyzed which address the above mentioned issues related to diffusion. The effect of mechanical dispersion is taken up in section 5 including presentation and discussion of the numerical results which address dispersive effects mentioned above. We summarize succinctly the results on diffusive (without mechanical dispersion) and dispersive effects in section 6. Finally we conclude in section 7. For the reader's convenience, we include a list of symbols and relations in Appendix-A.

2 Preliminaries

We consider two-dimensional fluid flows in a three-layer homogeneous porous media (see Figure 1) within Hele-Shaw model meaning the interfaces are treated as immiscible and Darcy's law is allowed to hold as in flows in a Hele-Shaw cell. In the leftmost layer, $-\infty < x \leq -L$, the fluid has a constant viscosity μ_l. The rightmost layer extends from $x = 0$ up to $x = \infty$ and is characterized by constant viscosity μ_r. The middle layer is of length L and contains a fluid of variable viscosity $\mu(x)$ such that $\mu_l \leq \mu(x) \leq \mu_r$. The fluid in this middle layer is immiscible with the fluids in the other two layers. For the purpose of application to EOR by chemical flooding, this fluid may be taken to be a polysolution (an aqueous phase containing polymer) having a concentration profile of polymer. The right interface, separating the middle and the right-most fluid layers, has an interfacial tension T_0, and the left interface, separating the middle and the left-most fluid layers, has an interfacial tension T_1. The fluid upstream at $x = -\infty$ has a velocity $(U, 0)$. The governing equations are the continuity equation, Darcy's law, and, assuming no mechanical dispersion, an advection-diffusion equation for the concentration of polymer.

$$\nabla \cdot \mathbf{u} = 0, \tag{1}$$

$$\nabla\, p = -\frac{\mu}{K}\, \mathbf{u}, \tag{2}$$

$$\frac{\partial c}{\partial t} + \mathbf{u} \cdot \nabla c = D_0 \triangle\, c, \tag{3}$$

where $\nabla = (\frac{\partial}{\partial x}, \frac{\partial}{\partial y})$, $\triangle$ is the Laplacian in the plane, c is the concentration of polymer in the middle layer, K is the permeability, and D_0, the diffusion coefficient, is a constant. For Hele-Shaw flows, $K = b^2/12$ where b is the width of the gap between the plates.

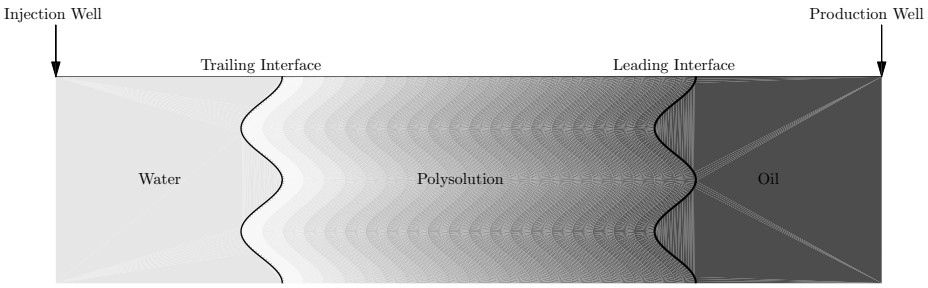

Figure 1: Polymer Flooding

Both interfaces are governed by both kinematic and dynamic boundary conditions. However, we consider

two different conditions for the concentration of polymer at the interfaces. First, we will consider a no-flux boundary condition at the interfaces, which is appropriate if the interfaces are **impermeable**. Then, we will consider Dirichlet boundary conditions in which the concentration of polymer is held constant at each interface. Such an interface would necessarily need to be **permeable**, allowing the proper amount of polymer to flow through each interface to keep the concentration fixed. For simplicity, we will henceforth refer to these interface conditions as **permeable** and **impermeable** even though the term **permeable** in itself does not imply that the concentration of polymer is fixed at each interface.

2.1 Impermeable Interfaces

First, we develop the stability equations for the case of no-flux boundary conditions. The above system (1)-(3) admits a simple basic solution, namely the whole fluid set-up moves with speed U in the x direction and the two interfaces, namely the one separating the left layer from the middle-layer and the other separating the right layer from the middle-layer, are planar, i.e. parallel to the y-axis. The concentration profile in the middle layer is taken to be a function of x only and satisfies equation (3). The pressure corresponding to this basic solution is obtained by integrating (2). In a frame moving with velocity $(U, 0)$, the set-up corresponding to the above basic solution is stationary along with two planar interfaces separating these three fluid layers. Here and below, with slight abuse of notation, the same variable x is used to refer to the $x-$coordinate in the moving reference frame. This is also necessary in order to preserve continuity of notation used in [12] and [13] which facilitates comparison of results obtained in this paper (which has diffusion) with those in [13] (which has no diffusion).

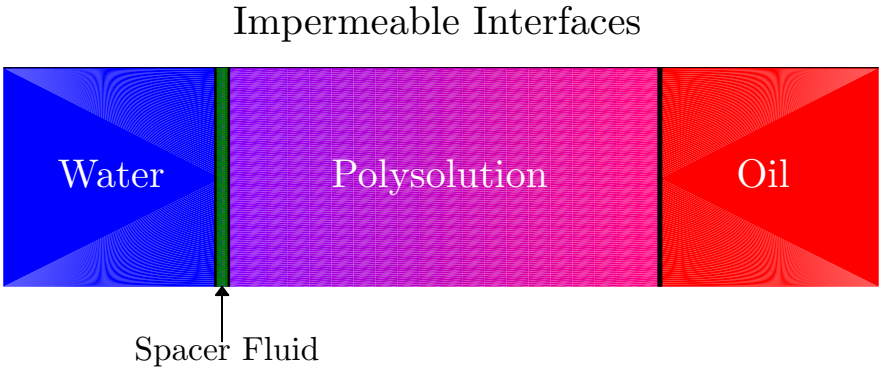

Figure 2: Impermeable Interfaces: Zero Neumann boundary condition for concentration of polymer at the interfaces

We scale the variables by the characteristic length L and the characteristic velocity U. Additionally, we scale the viscosity by the viscosity, μ_r, of the leading fluid.. With a slight abuse of notation, below we use the same notations for dimensionless variables as for dimensional variables. The dimensionless system in the

moving frame is

$$\left.\begin{array}{l} \nabla\cdot\mathbf{u} = 0, \\ \nabla p = -\frac{\mu}{K^*}\,\mathbf{u} - \frac{\mu}{K^*}\,\hat{i}, \\ \frac{\partial c}{\partial t} + \mathbf{u}\cdot\nabla c = \frac{1}{Pe}\triangle c, \\ \frac{\partial \eta}{\partial t} = \mathbf{u}\cdot\hat{n}, \\ [p] = -\frac{1}{Ca}\frac{T}{T_0}(\nabla\cdot\hat{n}), \\ \frac{\partial c}{\partial n} = 0, \end{array}\right\} \tag{4}$$

with interfaces at $x = -1$ and $x = 0$ where $Pe = UL/D_0$, $Ca = U\mu_r/T_0$, $K^* = K/L^2$, $x = \eta(y,t)$ is the position of an interface, T is the interfacial tension at the interface, $[p]$ denotes the jump in pressure across the interface, $\hat{n}$ is the normal vector to the interfaces, and $\partial/\partial n$ is the normal derivative across the interface. Equations $(4)_1$ through $(4)_3$ hold in $-1 < x < 0$ and $(4)_4$ through $(4)_6$ hold at each of the two interfaces with interfacial tension $T = T_0$ at $x = 0$ and $T = T_1$ at $x = -1$.

The basic solution to (4) is $(u = 0, v = 0, p_0(x,t), c_0(x,t))$, where $p_0(x,t)$ is obtained by integrating $(4)_2$. The interfaces remain planar at $x = -1$ and $x = 0$. We take the initial condition for the concentration profile, $c_0(x,0)$, to be a linear function. This is for easy comparison with the case of Dirichlet boundary conditions, as will be evident later (see section 2.2). For $t > 0$, the basic concentration profile is governed by the following problem

$$\left.\begin{array}{l} \frac{\partial c_0}{\partial t} = \frac{1}{Pe}\frac{\partial^2 c_0}{\partial x^2}, \\ \frac{\partial c_0}{\partial x} = 0, \quad x = -1, 0. \end{array}\right\}$$

Through separation of variables, the solution to this equation can be written as

$$c_0(x,t) = a_0 + \sum_{n=1}^{\infty} a_n cos(n\pi x) e^{-\frac{1}{Pe}n^2\pi^2 t}, \tag{5}$$

where the coefficients a_n come from expanding the initial condition in terms of a cosine series

$$c_0(x,0) = a_0 + \sum_{n=1}^{\infty} a_n cos(n\pi x).$$

The viscosity μ inside the middle layer is a function of concentration. We denote $\mu_0 = \mu(c_0)$. We perturb this basic solution by $(\widetilde{u}, \widetilde{v}, \widetilde{p}, \widetilde{c})$. We decompose the disturbances into fourier modes in the y-direction and write them as

$$(\widetilde{u}, \widetilde{v}, \widetilde{p}, \widetilde{c}) = (f(x,t), \psi(x,t), \phi(x,t), h(x,t))\, e^{i\,k\,y}. \tag{6}$$

Using this ansatz in equations $(4)_1 - (4)_3$,

$$-\frac{\partial}{\partial x}\left(\mu_0\frac{\partial f}{\partial x}\right) + k^2\mu_0 f = -k^2\frac{d\mu_0}{dc}h, \tag{7}$$

and

$$\frac{\partial h}{\partial t} = -\frac{\partial c_0}{\partial x}f + \frac{1}{Pe}\left(\frac{\partial^2 h}{\partial x^2} - k^2 h\right). \tag{8}$$

We now investigate the boundary conditions of the eigenvalue problem given by (7) and (8). Consider a planar interface at $x = x_0$ that is perturbed by $\widetilde{\eta}(y,t)$. Using the boundary condition $(4)_4$, linearizing about the disturbances, and using the ansatz (6)

$$\frac{\partial \widetilde{\eta}}{\partial t} = f(x_0,t)e^{i\,k\,y}. \tag{9}$$

Using the linearized form of the boundary condition $(4)_5$ and the ansatz (6)

$$-\frac{\mu_0^+(x_0,t)}{k^2}\frac{\partial f^+(x_0,t)}{\partial x}e^{i\,k\,y}+\frac{\mu_0^-(x_0,t)}{k^2}\frac{\partial f^-(x_0,t)}{\partial x}e^{i\,k\,y}-\left(\mu_0^+(x_0,t)-\mu_0^-(x_0,t)\right)\widetilde{\eta}=\frac{K^*}{Ca}\frac{T}{T_0}\widetilde{\eta}_{yy}, \tag{10}$$

where the superscripts '+' and '−' denote the limits from the left and the right, respectively. We first investigate this interface condition at $x_0=-1$. Integrating (9), we have $\widetilde{\eta}=A(t)e^{i\,k\,y}$ where

$$\frac{dA}{dt}=f(-1,t). \tag{11}$$

Using (11) in (10) and taking into account the far-field boundary condition at $x=-\infty$,

$$\mu_0^+(-1,t)\frac{\partial f^+(-1,t)}{\partial x}=\mu_l k\frac{dA}{dt}-E_1A(t), \tag{12}$$

where

$$E_1=k^2\left(\mu_0^+(-1,t)-\mu_l\right)-k^4\frac{K^*}{Ca}\frac{T_1}{T_0}. \tag{13}$$

For the interface condition at $x_0=0$, we integrate (9) and get $\widetilde{\eta}=B(t)e^{i\,k\,y}$ where

$$\frac{dB}{dt}=f(0,t). \tag{14}$$

Using (14) in (10),

$$-\mu_0^-(0,t)\frac{\partial f^-(0,t)}{\partial x}=\mu_r k\frac{dB}{dt}-E_0B(t), \tag{15}$$

where

$$E_0=k^2\left(\mu_r-\mu(0)\right)-k^4\frac{K^*}{Ca}. \tag{16}$$

If the interfaces are impermeable, there is a no flux condition for the concentration of polymer at the interfaces. Recall that this is given by

$$\frac{\partial c}{\partial n}=0,\qquad x=x_0+\widetilde{\eta}.$$

Using the ansatz (6) and the expression for $\widetilde{\eta}$ at each interface and linearizing with respect to the disturbances,

$$\left.\begin{array}{l}\frac{\partial h(-1,t)}{\partial x}=-A(t)\frac{\partial^2 c_0(-1,t)}{\partial x^2}\\ \frac{\partial h(0,t)}{\partial x}=-B(t)\frac{\partial^2 c_0(0,t)}{\partial x^2}\end{array}\right\} \tag{17}$$

Collecting equations (7), (8), (12), (15), and (17), the system of equations for impermeable interfaces is

$$\left.\begin{array}{ll}-\frac{\partial}{\partial x}\left(\mu\frac{\partial f}{\partial x}\right)+k^2\mu f=-k^2\frac{d\mu}{dc}h, & x\in(-1,0),\\ \frac{\partial h}{\partial t}=-\frac{\partial c}{\partial x}f+\frac{1}{Pe}\left(\frac{\partial^2 h}{\partial x^2}-k^2h\right), & x\in(-1,0),\\ \mu(-1,t)\frac{\partial f(-1,t)}{\partial x}=\mu_l k\frac{dA}{dt}-E_1A(t),\\ -\mu(0,t)\frac{\partial f(0,t)}{\partial x}=\mu_r k\frac{dB}{dt}-E_0B(t),\\ \frac{\partial h(-1,t)}{\partial x}=-A(t)\frac{\partial^2 c(-1,t)}{\partial x^2},\\ \frac{\partial h(0,t)}{\partial x}=-B(t)\frac{\partial^2 c(0,t)}{\partial x^2}.\end{array}\right\} \tag{18}$$

Note that equations $(18)_1$ and $(18)_2$ depend on time through μ and c. We have dropped the subscript '0' from μ and c, and we have dropped all superscripts.

If at some fixed time t, there is a number $\sigma(t)$ such that the functions $h(x,t)$, $A(t)$, and $B(t)$ satisfy

$$\left.\begin{array}{l} \frac{\partial h(x,t)}{\partial t} = \sigma(t)h(x,t), \\ \frac{dA}{dt} = \sigma(t)A(t), \\ \frac{dB}{dt} = \sigma(t)B(t), \end{array}\right\} \tag{19}$$

then by plugging (19) into (18), (f,h,σ) is a solution to the following eigenvalue problem:

$$\left.\begin{array}{ll} -\frac{\partial}{\partial x}\left(\mu\frac{\partial f}{\partial x}\right) + k^2\mu f = -k^2\frac{d\mu}{dc}h, & x \in (-1,0), \\ -\frac{\partial c}{\partial x}f + \frac{1}{Pe}\left(\frac{\partial^2 h}{\partial x^2} - k^2 h\right) = \sigma h, & x \in (-1,0), \\ \mu(-1,t)\frac{\partial f(-1,t)}{\partial x} = \left(\mu_l k - \frac{E_1}{\sigma}\right) f(-1,t), & \\ -\mu(0,t)\frac{\partial f(0,t)}{\partial x} = \left(\mu_r k - \frac{E_0}{\sigma}\right) f(0,t), & \\ \frac{\partial h(-1,t)}{\partial x} = -\frac{1}{\sigma}\frac{\partial^2 c(-1,t)}{\partial x^2} f(-1,t), & \\ \frac{\partial h(0,t)}{\partial x} = -\frac{1}{\sigma}\frac{\partial^2 c(0,t)}{\partial x^2} f(0,t). & \end{array}\right\} \tag{20}$$

Therefore, the eigenvalues of the system (20) are the time-dependent growth rates of the disturbances for our problem.

2.2 Permeable Interfaces

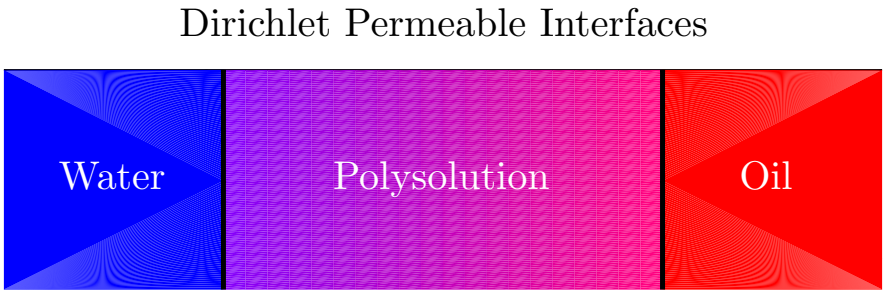

Figure 3: Dirichlet Permeable Interfaces: concentration of polymer at each of the two interfaces in the middle layer is held fixed.

We now consider the case in which the concentration of polymer is fixed at each interface. This condition is given by

$$c = b_i, \qquad i = 1,2 \tag{21}$$

where b_i is a constant for each interface. A main difference between this case and the previous one is that this boundary condition admits a basic solution which is steady. In particular, the fluid moves with speed U in the positive x direction, the fluid interfaces are planar, and the concentration of polymer is a **linear** function. In this case, the analysis above holds for equations $(20)_1$, $(20)_2$, $(20)_3$, and $(20)_4$. However, equations $(20)_5$ and $(20)_6$ no longer hold. The corresponding boundary conditions using equation (21) at each interface are

$$\left.\begin{array}{l} h(-1) = \frac{a}{\sigma}f(-1) \\ h(0) = \frac{a}{\sigma}f(0), \end{array}\right\} \tag{22}$$

where $a = b_2 - b_1$.

The eigenvalue problem that governs the stability for fixed concentration on the boundaries is then given by

$$\left.\begin{array}{ll} -\frac{d}{dx}\left(\mu\frac{df}{dx}\right)+k^2\mu f=-k^2\frac{d\mu}{dc}h, & x\in(-1,0),\\ -af+\frac{1}{Pe}\left(\frac{d^2h}{dx^2}-k^2h\right)=\sigma h, & x\in(-1,0),\\ \mu(-1)\frac{df}{dx}(-1)=\left(\mu_l\,k-\frac{E_1}{\sigma}\right)f(-1),\\ -\mu(0)\frac{df}{dx}(0)=\left(\mu_r\,k-\frac{E_0}{\sigma}\right)f(0),\\ h(-1)=\frac{a}{\sigma}f(-1)\\ h(0)=\frac{a}{\sigma}f(0). \end{array}\right\} \tag{23}$$

Note that in this case, the function μ does not depend on time because the basic solution is steady. Therefore, the system is autonomous and the eigenvalue σ does not depend on time. Taking into consideration equation (19), the disturbances will grow exponentially proportional to $e^{\sigma t}$.

3 Fourth order eigenvalue problem

It is often convenient, both numerically and analytically, to eliminate the function h from the system (20) or (23) and consider a single equation for the function f. This equation depends on the relationship between the viscosity μ and the concentration of polymer c. We assume that μ is a linear function of c, which is reasonable to assume for small c. This assumption was made implicitly in [14] and [15], but we make this dependence explicit here. We do this process for both sets of boundary conditions.

3.1 Impermeable Interfaces

We start by considering the case of no-flux boundary conditions. Solving equation $(20)_1$ for h,

$$h=\frac{1}{k^2\frac{d\mu}{dc}}\left(\mu\frac{\partial^2 f}{\partial x^2}+\frac{\partial\mu}{\partial x}\frac{\partial f}{\partial x}-k^2\mu f\right). \tag{24}$$

Plugging (24) into $(20)_2$ and denoting $\lambda=1/\sigma$, we arrive at the fourth order eigenvalue problem

$$\begin{aligned} &Pe\left(\mu\frac{\partial^2 f}{\partial x^2}+\frac{\partial\mu}{\partial x}\frac{\partial f}{\partial x}-k^2\mu f\right)\\ =&\lambda\left\{\mu\frac{\partial^4 f}{\partial x^4}+3\frac{\partial\mu}{\partial x}\frac{\partial^3 f}{\partial x^3}+\left(3\frac{\partial^2\mu}{\partial x^2}-2k^2\mu\right)\frac{\partial^2 f}{\partial x^2}+\left(\frac{\partial^3\mu}{\partial x^3}-3k^2\frac{\partial\mu}{\partial x}\right)\frac{\partial f}{\partial x}-k^2\left(\frac{\partial^2\mu}{\partial x^2}+Pe\frac{\partial\mu}{\partial x}-k^2\mu\right)f\right\}. \end{aligned} \tag{25}$$

Note that in the limit $Pe\to\infty$, this becomes

$$\mu\frac{\partial^2 f}{\partial x^2}+\frac{\partial\mu}{\partial x}\frac{\partial f}{\partial x}-k^2\mu f=-\lambda k^2\frac{\partial\mu}{\partial x}f. \tag{26}$$

This is the non-dimensional form of the equation derived in the absence of diffusion in [4].

Four boundary conditions are necessary for this fourth-order eigenvalue problem. Two of them are $(20)_3$ and $(20)_4$. The other two come from $(20)_5$ and $(20)_6$. Using the expression (24) in the boundary condition $(20)_5$,

$$\begin{aligned} &\mu(-1)\frac{\partial^3 f}{\partial x^3}(-1)+2\frac{\partial\mu}{\partial x}(-1)\frac{\partial^2 f}{\partial x^2}(-1)+\left(\frac{\partial^2\mu}{\partial x^2}(-1)-k^2\mu(-1)\right)\frac{\partial f}{\partial x}(-1)-k^2\frac{\partial\mu}{\partial x}(-1)f(-1)\\ =&-\lambda k^2\frac{\partial^2\mu}{\partial x^2}(-1)f(-1). \end{aligned} \tag{27}$$

Likewise, using the expression (24) in the boundary condition $(20)_6$, we get

$$\mu(0)\frac{\partial^3 f}{\partial x^3}(0) + 2\frac{\partial \mu}{\partial x}(0)\frac{\partial^2 f}{\partial x^2}(0) + \left(\frac{\partial^2 \mu}{\partial x^2}(0) - k^2\mu(0)\right)\frac{\partial f}{\partial x}(0) - k^2\frac{\partial \mu}{\partial x}(0)f(0) = -\lambda k^2\frac{\partial^2 \mu}{\partial x^2}(0)f(0). \tag{28}$$

Collecting equations (25), $(20)_3$, $(20)_4$, (27), and (28),

$$\left.\begin{array}{l} Pe\left(\mu\frac{\partial^2 f}{\partial x^2} + \frac{\partial \mu}{\partial x}\frac{\partial f}{\partial x} - k^2\mu f\right) \\ = \lambda\left\{\mu\frac{\partial^4 f}{\partial x^4} + 3\frac{\partial \mu}{\partial x}\frac{\partial^3 f}{\partial x^3} + \left(3\frac{\partial^2 \mu}{\partial x^2} - 2k^2\mu\right)\frac{\partial^2 f}{\partial x^2} + \left(\frac{\partial^3 \mu}{\partial x^3} - 3k^2\frac{\partial \mu}{\partial x}\right)\frac{\partial f}{\partial x} - k^2\left(\frac{\partial^2 \mu}{\partial x^2} + Pe\frac{\partial \mu}{\partial x} - k^2\mu\right) f\right\}, \\ \mu(-1)\frac{\partial f}{\partial x}(-1) = (\mu_l\, k - \lambda E_1)\, f(-1), \\ -\mu(0)\frac{\partial f}{\partial x}(0) = (\mu_r\, k - \lambda E_0)\, f(0), \\ \mu(-1)\frac{\partial^3 f}{\partial x^3}(-1) + 2\frac{\partial \mu}{\partial x}(-1)\frac{\partial^2 f}{\partial x^2}(-1) + \left(\frac{\partial^2 \mu}{\partial x^2}(-1) - k^2\mu(-1)\right)\frac{\partial f}{\partial x}(-1) - k^2\frac{\partial \mu}{\partial x}(-1)f(-1) = -\lambda k^2\frac{\partial^2 \mu}{\partial x^2}(-1)f(-1), \\ \mu(0)\frac{\partial^3 f}{\partial x^3}(0) + 2\frac{\partial \mu}{\partial x}(0)\frac{\partial^2 f}{\partial x^2}(0) + \left(\frac{\partial^2 \mu}{\partial x^2}(0) - k^2\mu(0)\right)\frac{\partial f}{\partial x}(0) - k^2\frac{\partial \mu}{\partial x}(0)f(0) = -\lambda k^2\frac{\partial^2 \mu}{\partial x^2}(0)f(0). \end{array}\right\} \tag{29}$$

3.2 Permeable Interfaces

For fixed concentration of polymer at the interfaces, there are two major changes from the previous case. The first change is the last two boundary conditions, $(29)_4$ and $(29)_5$. The corresponding boundary conditions are found by using the expression (24) in the equations given by $(23)_5$ and $(23)_6$. This gives

$$\mu(-1)\frac{d^2 f}{dx^2}(-1) = \left[k^2\mu(-1) - \frac{\frac{d\mu}{dx}}{\mu(-1)}\left(\mu_l\, k - \lambda E_1\right) + \lambda k^2\frac{d\mu}{dx}\right] f(-1), \tag{30}$$

and

$$\mu(0)\frac{d^2 f}{dx^2}(0) = \left[k^2\mu(0) + \frac{\frac{d\mu}{dx}}{\mu(0)}\left(\mu_r\, k - \lambda E_0\right) + \lambda k^2\frac{d\mu}{dx}\right] f(0). \tag{31}$$

The second change from the previous case is that the function $\mu(x)$ is linear, since we assumed μ is a linear function of c and the basic concentration profile is linear. Therefore, all higher derivatives of μ in equation (29) are zero. Therefore, the eigenvalue problem which governs the growth rate of disturbances is

$$\left.\begin{array}{l} Pe\left(\mu\frac{d^2 f}{dx^2} + \frac{d\mu}{dx}\frac{df}{dx} - k^2\mu f\right) \\ = \lambda\left\{\mu\frac{d^4 f}{dx^4} + 3\frac{d\mu}{dx}\frac{d^3 f}{dx^3} - 2k^2\mu\frac{d^2 f}{dx^2} - 3k^2\frac{d\mu}{dx}\frac{df}{dx} - k^2\left(Pe\frac{d\mu}{dx} - k^2\mu\right) f\right\}, \\ \mu(-1)\frac{df}{dx}(-1) = (\mu_l\, k - \lambda E_1)\, f(-1), \\ -\mu(0)\frac{df}{dx}(0) = (\mu_r\, k - \lambda E_0)\, f(0), \\ \mu(-1)\frac{d^2 f}{dx^2}(-1) = \left[k^2\mu(-1) - \frac{\frac{d\mu}{dx}}{\mu(-1)}\left(\mu_l\, k - \lambda E_1\right) + \lambda k^2\frac{d\mu}{dx}\right] f(-1), \\ \mu(0)\frac{d^2 f}{dx^2}(0) = \left[k^2\mu(0) + \frac{\frac{d\mu}{dx}}{\mu(0)}\left(\mu_r\, k - \lambda E_0\right) + \lambda k^2\frac{d\mu}{dx}\right] f(0). \end{array}\right\} \tag{32}$$

4 Results and Discussion

In order to investigate the stabilizing effect of diffusion, computations are performed with various values of parameters which can be found in various figure captions below. For certain parameters, their values are kept fixed in all simulations. These are $\mu_l = 0.2$, $\mu_r = 1$, $Ca = 10^{-3}$, $K^* = 10^{-4}$, and $T_1/T_0 = 1$. Computations have also been performed with other values of these parameters but the conclusions that follow remain unchanged. In the following section, σ_{max} refers to the maximum growth rate over all wavenumbers, k. All computations are done using a pseudo-spectral method. Details of the numerical method as well as some results related to its validation can be found in Appendix B.

4.1 The Case of Fixed Concentration on the Interfaces (Permeable Interfaces)

First, we consider the numerical results obtained using the condition of fixed concentration of polymer on the interfaces. We start with this case because the results are simpler to explore due to the time independence of the eigenvalue problem. In keeping with the assumptions of [14] and [15], we assume that μ is a linear function of c, which is reasonable in the dilute regime. We have also considered the case in which μ depends exponentially on c, as is done in [27] and [28], but have found that the general trends and conclusions remain the same. Therefore, we only present the results for a linear relationship between viscosity and concentration of polymer. Since μ is a linear function of c and the basic concentration profile is a linear function of x, μ is also a linear function of x.

The system (32) is solved for the eigenvalues λ. The eigenvalues are then inverted to find $\sigma = 1/\lambda$. The values of σ computed in this case could be complex, but we are interested only in the real part, σ_R, which measures the growth rate of disturbances. Below, all references to growth rate mean the real part σ_R of σ and these are denoted by σ itself, with slight abuse of notation. Note that for each wavenumber k, there are an infinite number of eigenvalues and therefore an infinite number of values of σ. For the purpose of linear stability analysis, we are mainly concerned with the largest value of σ_R for each wavenumber. Therefore, all figures below include only plots of the largest σ_R for each k. $\sigma_{\max}$ below in the narrative or figures means the maximum value of σ_R with the maximum taken over all eigenvalues and all wavenumbers. Also, we refer to small values of Peclet number Pe (large values of the diffusion coefficient D_0) as strong diffusion and large values of Pe (small values of D_0) as mild diffusion.

The maximum growth rate $\sigma_{max}(\mu(x), Pe)$ depends on the viscous profile $\mu(x)$ as well as on the Peclet number Pe. The linear viscous profile is characterized by two parameters, $\mu(0)$ and $\mu(-1)$ with the restriction $\mu_l \leq \mu(-1) \leq \mu(0) \leq \mu_r$. Keeping these two parameters fixed at values $\mu(-1) = 0.408$ and $\mu(0) = 0.552$, corresponding to the infinite Peclet number (zero diffusion) optimal profile (see Figure 9) having $\sigma_{max} = 0.36039$, σ_{max} is computed for different finite values of Pe. Figure 4a shows the plot of σ_{max} versus $1/Pe$ with the viscous profile above it. From this figure we conclude that the effect of the diffusive stabilization is monotonic. However, the decrease in σ_{max} is gradual in this case.

In order to see a more dramatic effect from diffusion, we consider viscous profiles with larger gradients. Figure 4b shows the plot of σ_{max} versus $1/Pe$ for $\mu(-1) = 0.36$ and $\mu(0) = 0.68$, and Figure 4c shows the plot of σ_{max} versus $1/Pe$ for an even steeper viscous profile with $\mu(-1) = 0.28$ and $\mu(0) = 0.92$. The '$*$' (red online) on the y-axis in Figure 4c denotes the value of σ_{max} in the absence of diffusion. Note that the decrease in σ_{max} as the strength of diffusion increases is much greater for larger viscous gradients. In fact, the flow is almost stable for $Pe < 35$ when $\mu(-1) = 0.28$ and $\mu(0) = 0.92$.

One thing to note is that the plots in Figures 4b and 4c each have a point at which the slope of the curve is discontinuous. We will refer to this point as the turning point. In Figure 4b, the turning point is subtle, but is found inside the (blue online) circle. For figure 4c, it occurs when σ_{max} nears zero. We now investigate the turning point in order to shed light on the physical processes at play. Notice from the viscous profiles that in these two cases the jumps in viscosity at the interfaces are smaller than in Figure 4a, but the slope of the viscous profiles have increased. The first of these phenomena works to stabilize the flow while the second works to destabilize it.

To understand the contributions of the instability of the interfaces due to jumps in viscosity and the instability of the middle layer due to a viscous gradient in the layer, we consider three different sets of values

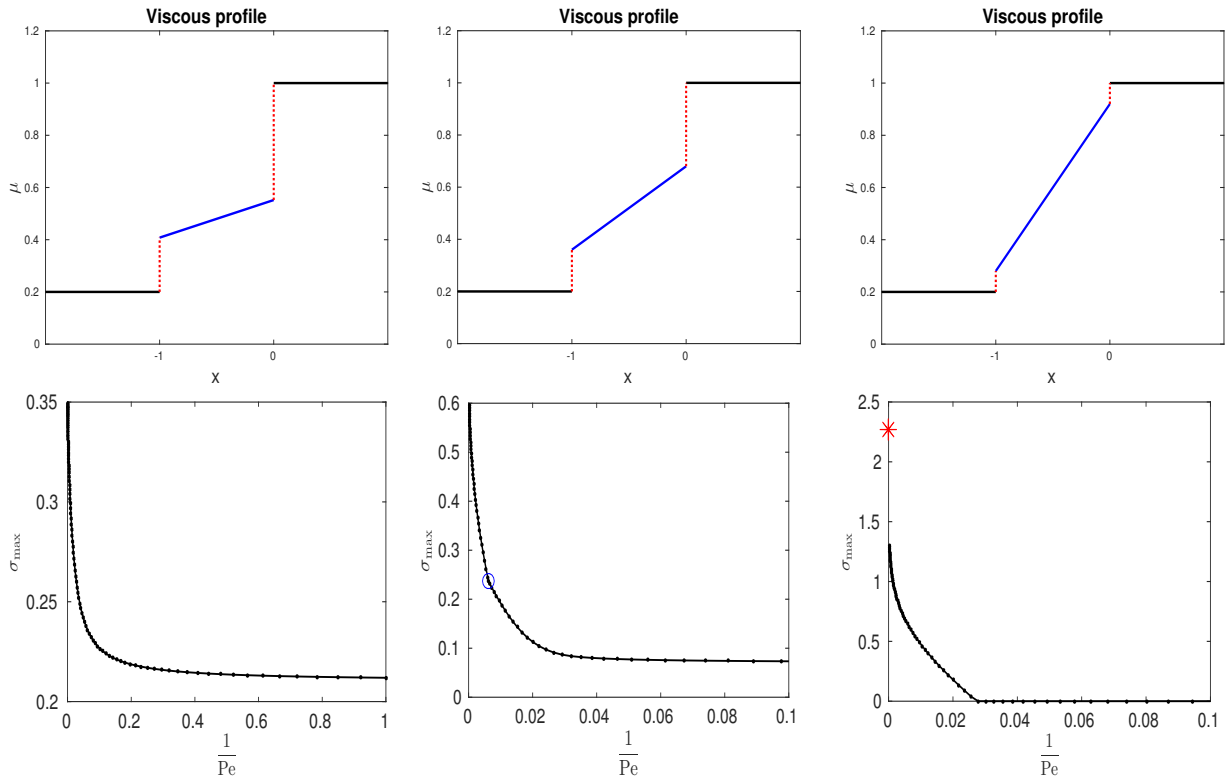

Figure 4: The case of permeable interfaces (with diffusion only): The maximum growth rate σ_{max} versus $1/Pe$ for: (a) $\mu(-1) = 0.408$ and $\mu(0) = 0.552$; (b) $\mu(-1) = 0.36$ and $\mu(0) = 0.68$; and (c) $\mu(-1) = 0.28$ and $\mu(0) = 0.92$. The '*' marker (red online) indicates the value of σ_{max} in the absence of diffusion. The corresponding viscous profiles are shown above each plot

.

for $\mu(-1)$ and $\mu(0)$ when there is no diffusion (i.e. $Pe = \infty$). Figure 5 shows plots of the maximum value of σ versus wavenumber k. Plot 5a uses the values $\mu(-1) = \mu(0) = 0.5040$. Therefore, the middle layer has constant viscosity and all of the instability comes from the interfaces. The viscosity jumps destabilize the flow while the interfacial tension stabilizes short waves. Plot 5b uses $\mu(-1) = 0.408$ and $\mu(0) = 0.552$, which correspond to the values in Figure 4a. The viscosity jumps are similar to those found in the constant viscosity case in Figure 5a, but there is now instability within the middle layer due to the viscous gradient in the layer. As we can see in Figure 5b, there is still a peak near $k = 1$, but, in contrast to Figure 5a, the short waves are not stable. In fact, as the wavenumber k increases to infinity, the value of σ in Figure 5b asymptotically approaches the dotted line. The new short wave behavior can be attributed to the middle layer instability. Finally, we consider plot 5c, which uses the values $\mu(-1) = 0.36$ and $\mu(0) = 0.68$, corresponding to Figure 4b. Like in Figures 5a and 5b, there is a local maximum near $k = 1$ which can be attributed to the instability of the interfaces. However, this is small compared to the short wave instability which comes from the middle layer. Because the viscosity increases more rapidly in the middle layer, the instability due to the middle layer is largest in this case.

When diffusion is added to the system, the growth rate decreases. However, the decrease is more pro-

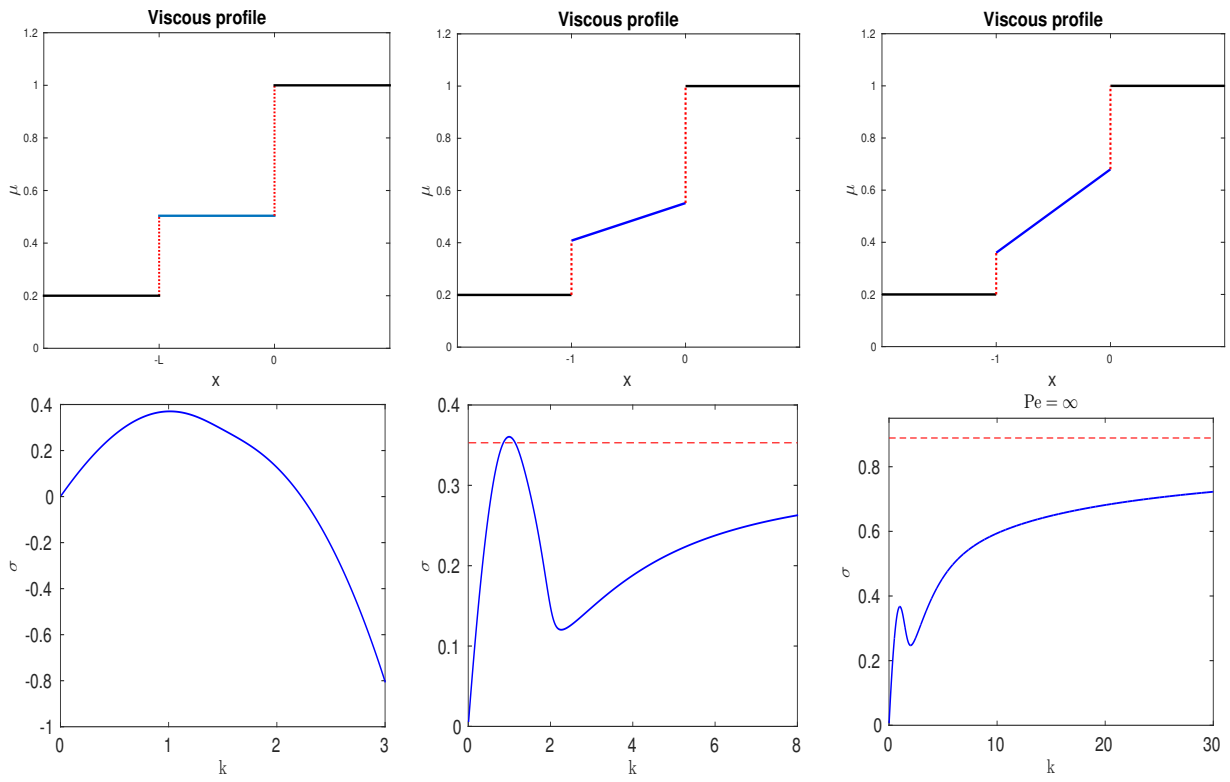

Figure 5: The case of permeable interfaces (with diffusion only): The maximum value of the growth rate σ for each wavenumber k is plotted versus k for several different values of $\mu(-1)$ and $\mu(0)$ when $Pe = \infty$. Plot shows $\mu(-1) = \mu(0) = 0.5040$. Plot (b) uses $\mu(-1) = 0.408$ and $\mu(0) = 0.552$. Plot (c) uses $\mu(-1) = 0.36$ and $\mu(0) = 0.68$. The dotted lines represent the limit of σ as $k \to \infty$.

nounced for short waves, due to the fact that the diffusion affects only the middle layer and not the interfaces. This effect is clearly illustrated by Figures 6 and 7. Figure 6 shows plots of the maximum value of σ versus k when $\mu(-1) = 0.408$ and $\mu(0) = 0.552$ for three different values of Pe. Recall that the plot for this viscous profile with $Pe = \infty$ is given in Figure 5b. Notice in Figure 5b that the large k limit is approximately equal to the peak near $k = 1$ (which is due to the interfacial instability). This balance is the reason this is the optimal viscous profile for $Pe = \infty$. Figure 6a uses $Pe = 1000$. Note that the peak near $k = 1$ remains and has only been slightly decreased. However, the short waves have now been stabilized by diffusion, adding a second maximum in the dispersion curve at a larger value of k. This behavior continues for Figures 6b and 6c which correspond to $Pe = 100$ and $Pe = 10$, respectively. The stabilization from diffusion is drastic for short waves, but mild for long waves.

This behavior shows why the case where the viscous profile is steeper is stabilized much more drastically by diffusion than when the profile is less steep. Figure 7 shows plots of the maximum value of σ versus k for the same three values of Pe but for a steeper profile with $\mu(-1) = 0.36$ and $\mu(0) = 0.68$. Recall from Figure 5c that the short wave instability of the middle layer dominates in the absence of diffusion. However, the addition of diffusion, even mild diffusion, stabilizes short enough waves, as we see in Figure 7a when $Pe = 1000$. Here, there is a second local maximum near $k = 9$ and this maximum value is already much

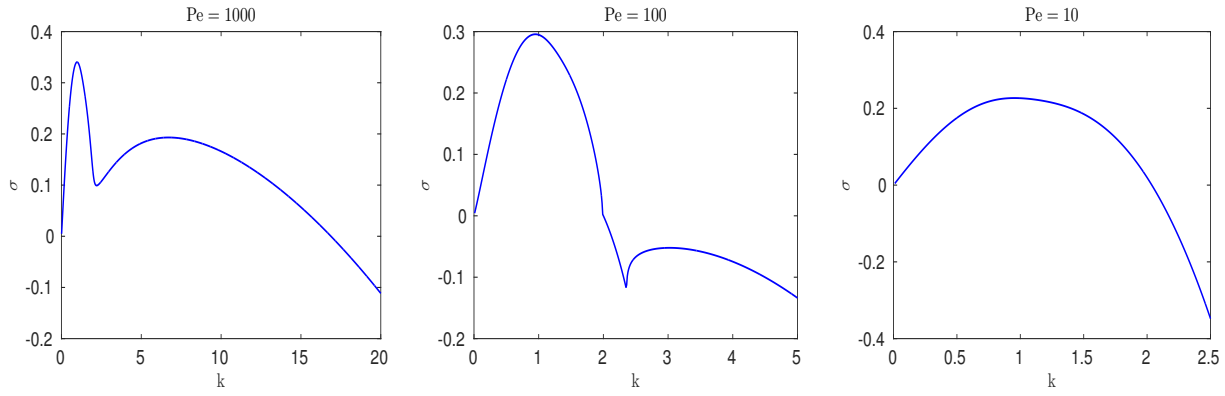

(a) (b) (c)

Figure 6: The case of permeable interfaces (with diffusion only): The maximum value of the growth rate σ for each wavenumber k is plotted versus k for $\mu(-1) = 0.408$ and $\mu(0) = 0.552$ and for several different values of Pe. Recall $\mu_l = 0.2$ and $\mu_r = 1$.

smaller than the large k limit for $Pe = \infty$ (given by the dotted line in Figure 5c). From Figures 7b and 7c, we see that as Pe decreases, the short waves become more stabilized until the local maximum that occurs due to the interfacial instability (long waves) overtakes the local maximum due to the middle layer instability (short waves). Figure 7c, which uses $Pe = 10$, shows the case when the interfacial instability dominates. This maximum is much smaller than the one in Figure 6c because the viscous jumps at the interfaces are much smaller in this case.

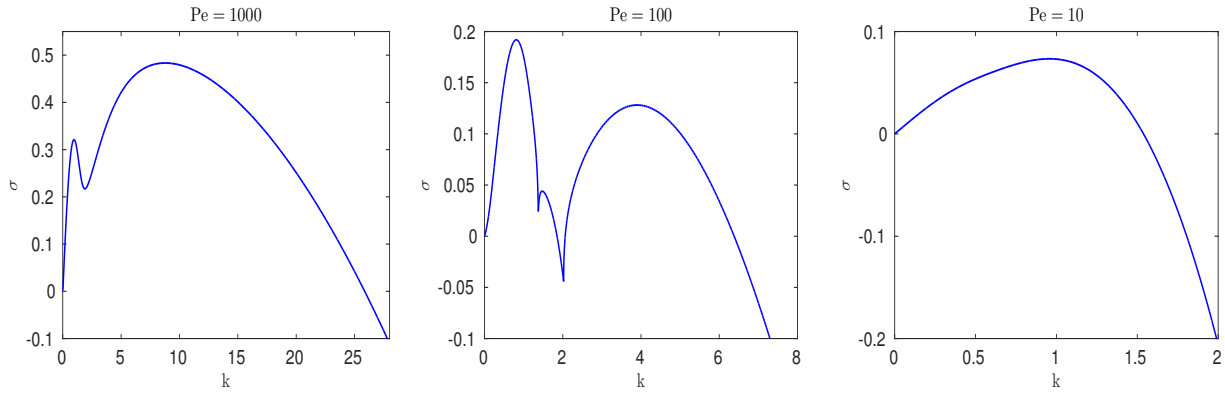

(a) (b) (c)

Figure 7: The case of permeable interfaces (with diffusion only) The maximum value of the growth rate σ for each wavenumber k is plotted versus k for $\mu(-1) = 0.36$ and $\mu(0) = 0.68$ and for several different values of Pe. Recall $\mu_l = 0.2$ and $\mu_r = 1$. This figure is similar to Figure 6 but with a different viscous profile.

The last issue to address with regards to this example is the turning point in the plot of Figure 4b. The turning point represents the point at which the diffusion has stabilized the middle layer so that the two local maxima are the same. For the case $\mu(-1) = 0.36$ and $\mu(0) = 0.68$ (the data used in Figure 4b), this occurs when $Pe = 161$. We plot the maximum value of σ versus k for this value of Pe in Figure 8.

The behavior that we have seen to this point shows that diffusion stabilizes flows with highly unstable

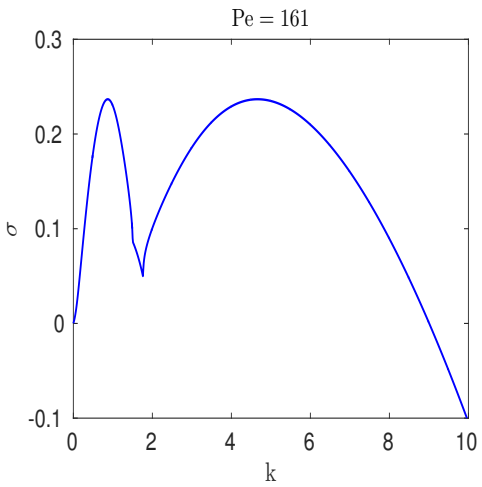

Figure 8: The case of permeable interfaces (with diffusion only): The maximum value of the growth rate σ for each wavenumber k is plotted versus k when $\mu(-1) = 0.36$ and $\mu(0) = 0.68$ and $Pe = 161$.

middle layers more than it stabilizes flows with highly unstable interfaces. Therefore, we expect that for larger diffusion, it would be advantageous to have flows that have a larger viscous gradient in order to minimize the instability of the interfaces. This is what we show next.

For any specific choice of Pe, σ_{max} is computed for all possible values of $\mu(-1)$ and $\mu(0)$, which characterize linear viscous profiles of the middle layer. The square grid mesh in Figure 9 (this is a color plot online) shows the maximum growth rate σ_{max} corresponding to $\mu(-1)$ and $\mu(0)$ for four values of the Peclet number Pe. The value of σ_{max} for each cell can be read from the color bar according to the color of the grid cell. The coordinates of each cell give the values $\mu(0)$ and $\mu(-1)$. The plot corresponding to $Pe = \infty$ shows that the optimal viscous profile in this case (recall this is $\mu(-1) = 0.408$ and $\mu(0) = 0.552$) has a relatively small viscous gradient in the middle layer. However, as diffusion increases, the optimal profile has a larger viscous gradient. For $Pe = 10$, the optimal profile has no viscous jump at the interfaces and the flow is almost completely stabilized by strong diffusion.

Using data from these simulations, the optimal profile for which the σ_{max} takes its minimum value is found for several values of Pe. Figure 10a shows the plot of σ_{max} versus $1/Pe$ for the optimal profiles. Compare this plot with Figures 4a, 4b, and 4c. Notice that choosing the optimal profile for a given value of Pe greatly increases the stabilizing effect of diffusion.

As mentioned above, as the diffusion increases, the slope of the optimal viscous profile also increases. To see this dependence, we plot the slope of the optimal viscous profile (given by $\mu(0) - \mu(-1)$) versus $1/Pe$ in Figure 10b. Note that, in general, the optimal viscous profile becomes more steep as the strength of diffusion increases. There is a small region in Figure 10b near $1/Pe = 0.015$ in which the slope of the viscous profile does not increase monotonically with the strength of diffusion. This goes against our expectations and we currently have no physical explanation. Also note that since $\mu(0) < \mu_r = 1$ and $0.2 = \mu_l < \mu(-1)$, the maximum value of the slope is 0.8. When $1/Pe > 0.04$, the optimal viscous profile takes on this value.

In order to determine the optimal viscous profile above, the value of σ_{max} has been found for all possible linear viscous profiles. In the absence of diffusion, some principles have been formed for determining the optimal viscous profile without an exhaustive search [8, 7, 10, 22]. In [8] and [10], selection principles for

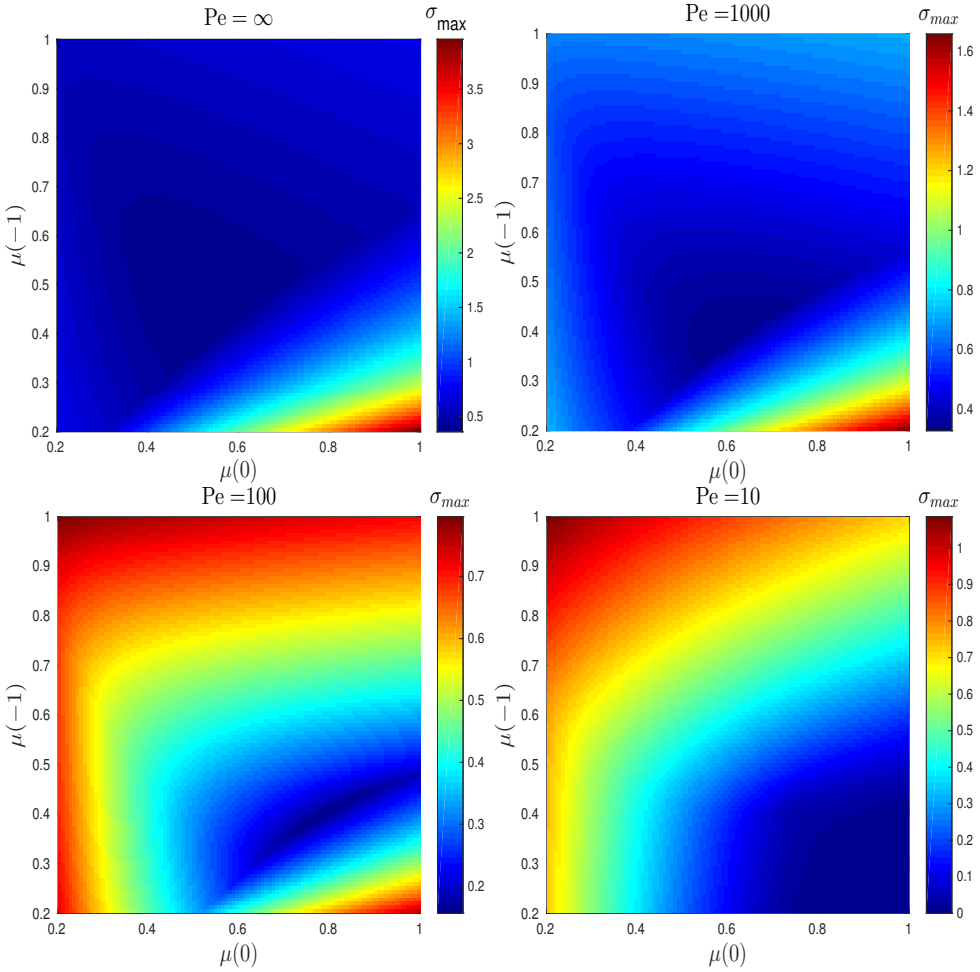

Figure 9: (Color plot online) The case of permeable interfaces (with diffusion only): The maximum growth rate σ_{max} versus $\mu(-1)$ and $\mu(0)$ for some different Peclet numbers. The other parameter values are $\mu_l = 0.2$, $\mu_r = 1$, $Ca = 10^{-3}$, $K^* = 10^{-4}$, and $T_1/T_0 = 1$.

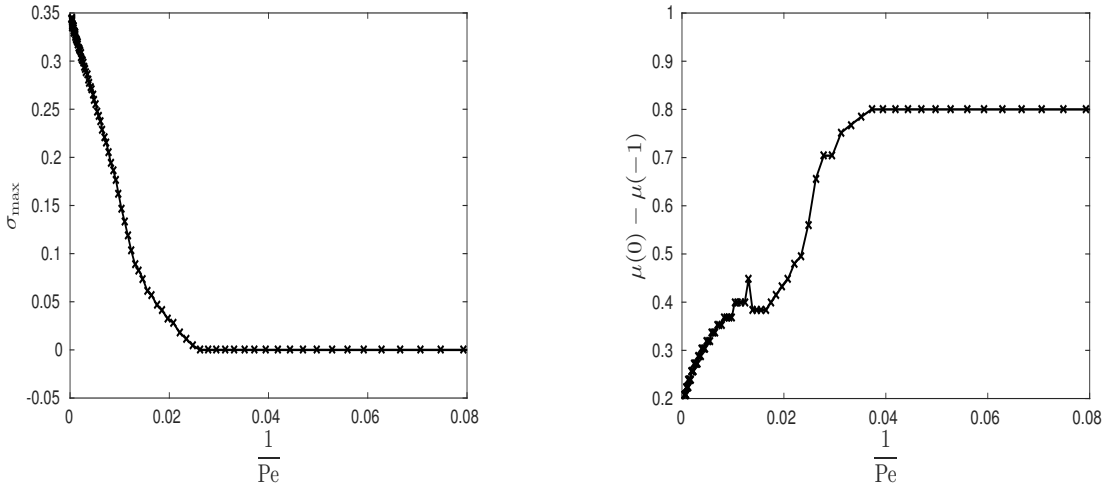

(a) (b)

Figure 10: The case of permeable interfaces (with diffusion only): (a) The maximum growth rate σ_{max} versus $1/Pe$ for optimal profiles. (b) The slope $\mu(0) - \mu(-1)$ of the optimal viscous profile versus $1/Pe$. The other parameter values are $\mu_l = 0.2$, $\mu_r = 1$, $Ca = 10^{-3}$, $K^* = 10^{-4}$, and $T_1/T_0 = 1$.

optimal viscous profiles are determined through a numerical study for three and four layer flows, respectively. In [7], a simple and fast method for choosing the optimal viscous profile is given based on upper bounds on the growth rate. In [22], a class of optimal viscous profiles are determined analytically under some additional assumptions. No similar results exist for determining the optimal viscous profile a priori in the present case. This is an open problem.

Regarding stability of three-layer immiscible flow to **infinitesimally small perturbations**, several interesting and useful inferences can be drawn from figures 4a, 4b, 4c, 9, 10a, and 10b such as (i) increasing the strength of diffusion increases the stabilization for the same viscous profile which may be considered by some as a classic result; (ii) significantly enhanced stabilization can be achieved by a proper choice of viscous profile without changing the Peclet number (compare Figure 4a and Figure 10a); (iii) even very mild diffusion can drastically stabilize an otherwise unstable flow provided the viscous profile is carefully chosen. In Figure 10a, we see that $\sigma_{max} \approx 0.05$ when $1/Pe \approx 0.017$ for the optimal viscous profile, an approximate seven-fold decrease from the same for the zero diffusion case resulting in a seven-fold gain in stabilization; (iv) there exists a range of viscous profiles for which the flow is almost completely stable, even for modest values of Peclet number (see the blue region in the bottom right corner of Figure 9 with $Pe = 10$); (v) at $1/Pe = 0.04$ (see Figure 10a), $\sigma_{max} \approx 0$ suggesting that the flow is neutrally stable to infinitesimal perturbations with a large enough value of diffusion and corresponding optimal viscous profile. However, the flow could still be unstable to **finite amplitude perturbations**.

4.2 The Case of No-Flux Through the Interfaces (Impermeable Interfaces)

Next, we consider the growth rate when the interfaces are impermeable. Recall that for impermeable interfaces, the viscous profile of the middle layer depends on time. We use a quasi-static approximation, i.e. we consider the stability with time t frozen at different time levels.

We start by investigating the effect of diffusion at time $t = 0$. In order to compare with the previous results, we consider an initially linear concentration profile. Since viscosity depends linearly on concentration, $\mu(x)$ is also a linear function. In Figure 11a, we plot σ_{max} versus $1/Pe$ for three different linear viscous profiles. Plots of the viscous profiles are found in Figure 11b. The solid line in Figure 11b corresponds to a viscous profile with $\mu(-1) = 0.408$ and $\mu(0) = 0.552$. In the absence of diffusion, this is the optimal viscous profile and was used in Figure 4a. Although difficult to see from the scale of Figure 11a, σ_{max} is a very slowly decreasing function of $1/Pe$. Therefore, increasing the strength of diffusion has a very mild stabilizing effect. However, just as in the previous section, diffusion has a dramatic effect for viscous profiles which have a large gradient and small viscous jumps at the interface. For example, the dotted line corresponds to a linear viscous profile with $\mu(-1) = .28$ and $\mu(0) = .92$. Here, $\sigma_{max} = 2.27149$ in the absence of diffusion, but σ_{max} is much smaller for even mild diffusion. The dashed line corresponds to a viscous profile with almost no jumps at the interfaces ($\mu(-1) = 0.2008$ and $\mu(0) = 0.9992$). For large enough diffusion, σ_{max} is almost zero.

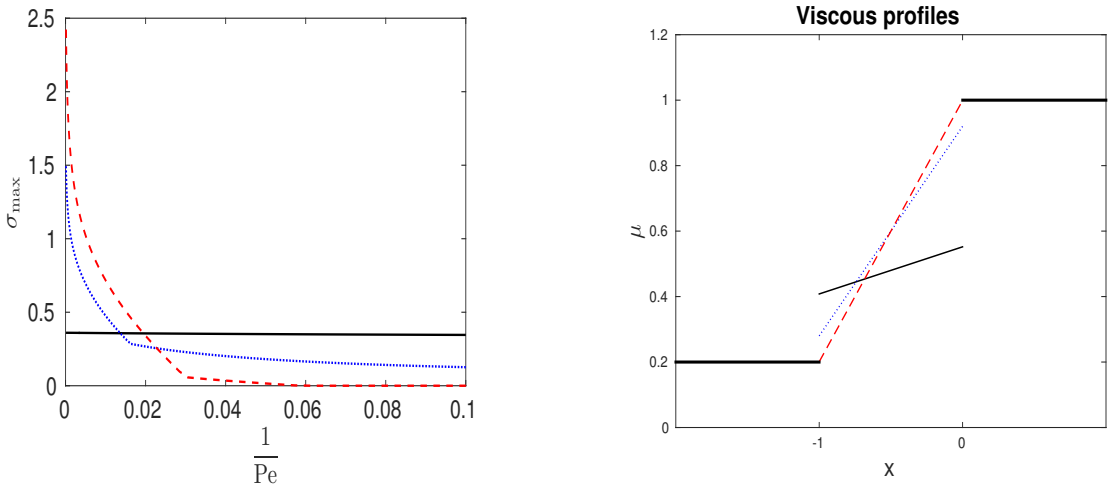

(a) (b)

Figure 11: The case of impermeable interfaces (with diffusion only): Plot (a) shows σ_{max} versus $1/Pe$ for three different viscous profiles at $t = 0$. The three profiles are plotted in (b). The solid line corresponds to a linear viscous profile with $\mu(-1) = 0.408$ and $\mu(0) = 0.552$. The dotted line corresponds to a linear viscous profile with $\mu(-1) = 0.28$ and $\mu(0) = 0.92$. The dashed line corresponds to a linear viscous profile with $\mu(-1) = 0.2008$ and $\mu(0) = 0.9992$. Other parameter values are $\mu_l = 0.2$, $\mu_r = 1$, $Ca = 10^{-3}$, $K^* = 10^{-4}$, and $T_1/T_0 = 1$.

As was done in the case of permeable interfaces, the optimal viscous profile for different values of Pe can be explored for time $t = 0$ in the case of impermeable interfaces. In Figure 12, the optimal linear viscous profiles are found for $Pe = 1000$, $Pe = 100$, and $Pe = 10$ by computing σ_{max} for all possible linear viscous profiles. Similar to the case of permeable interfaces, the optimal viscous profile is steeper when Pe is smaller. This is seen in Figure 12 by the fact that the minimal value of σ_{max} moves down and to the right as Pe is decreased. Note from the scale of σ_{max} in these plots that the value of σ_{max} for the optimal viscous profile when $Pe = 10$ is significantly smaller than the value of σ_{max} for the optimal viscous profile when $Pe = 1000$ or $Pe = 100$ which further demonstrates the strong stabilizing effect of diffusion.

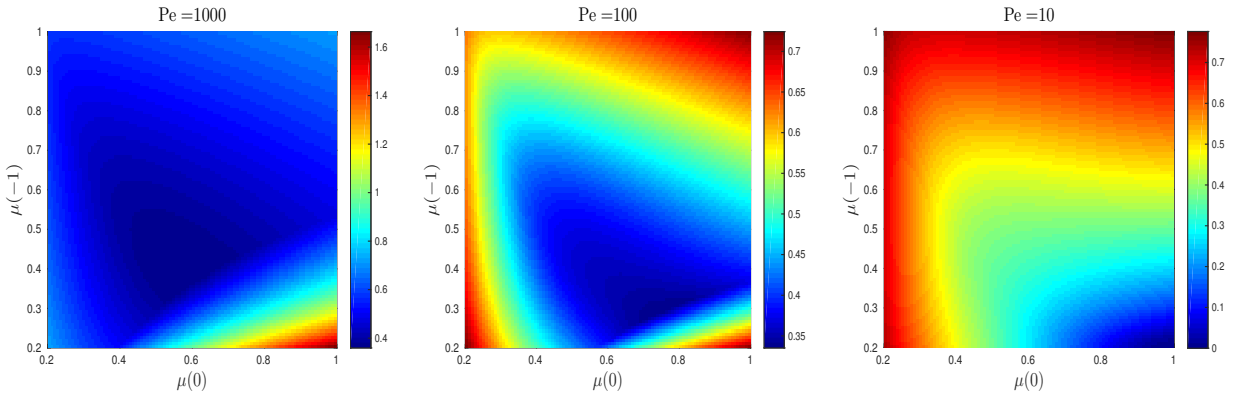

Figure 12: (Color plot online) The case of impermeable interfaces (with diffusion only): The maximum growth rate σ_{max} versus $\mu(-1)$ and $\mu(0)$ for some different Peclet numbers. The other parameter values are $\mu_l = 0.2$, $\mu_r = 1$, $Ca = 10^{-3}$, $K^* = 10^{-4}$, and $T_1/T_0 = 1$. This is a color figure.

Next, we consider the effect of diffusion over time. In order to simplify the results, we consider an initially linear viscous profile with $\mu(-1) = 0.28$ and $\mu(0) = 0.92$. As time elapses, the basic concentration profile evolves according to equation $(4)_3$. Since the viscosity depends linearly on the concentration, the viscous profile evolves accordingly. As is the case when $t = 0$, increasing the strength of diffusion results in a reduction in the growth rate for mild diffusion. However, in the presence of diffusion, the long-time limit of the initial concentration profile is a constant concentration profile, which leads to large viscous jumps at the interfaces. When diffusion is strong, the concentration approaches this limit more quickly. These competing effects result in a more complicated picture of the effect of diffusion at later times. In Figure 13a, σ_{max} is plotted versus $1/Pe$ for four different times. The beginning part of the dotted curve corresponding to $t = 0$ is a repeat of the dotted curve found in Figure 11a. In that case, σ_{max} is a strictly decreasing function of $1/Pe$, meaning that an increase in diffusion always makes the flow less unstable. However, for all other times, σ_{max} is a decreasing function when $1/Pe$ is small, but then σ_{max} achieves a global minimum for some value of Pe and thereafter σ_{max} becomes an increasing function of $1/Pe$ with a finite asymptotic limit. The optimal value of Pe, that is, the one which minimizes σ_{max}, is an increasing function of time. Based on the minimums of the curves in Figure 13a, the optimal value of Pe is 11.72 when $t = 0.5$, 16.92 when $t = 1$, and 28.82 when $t = 2$. The resulting viscous profiles obtained from using these optimal choices of Pe at each of the corresponding times are plotted in Figure 13b. So, for example, the solid curve is obtained by plotting the basic concentration profile at time $t = 0.5$ when $Pe = 11.72$. Although the strength of diffusion decreases for later times, the viscous profile is still less steep for later times.

Finally, we focus on one specific value of Pe and investigate the behavior of σ_{max} over time. We will again consider a basic concentration profile which is initially linear and results in an initial viscous profile with $\mu(-1) = 0.28$ and $\mu(0) = 0.92$. We use $Pe = 10$. Figure 14a shows σ_{max} plotted as a function of time. Recall that in the absence of diffusion, the maximum growth rate is given by the symbol '*' (red online) in Figure 4c (the value of which is $\sigma_{max} = 2.27149$). Clearly, diffusion has a large stabilizing effect. Figure 14b shows how the viscous profile evolves from time $t = 0$ to $t = 1$. Notice that as time increases, so do the jumps in viscosity at the interfaces, since $\mu_l = 0.2$ and $\mu_r = 1$. That leads to the increase in σ_{max} that we see in Figure 14a. In the limit $t \to \infty$, the viscous profile becomes constant. Since no polymer leaves the

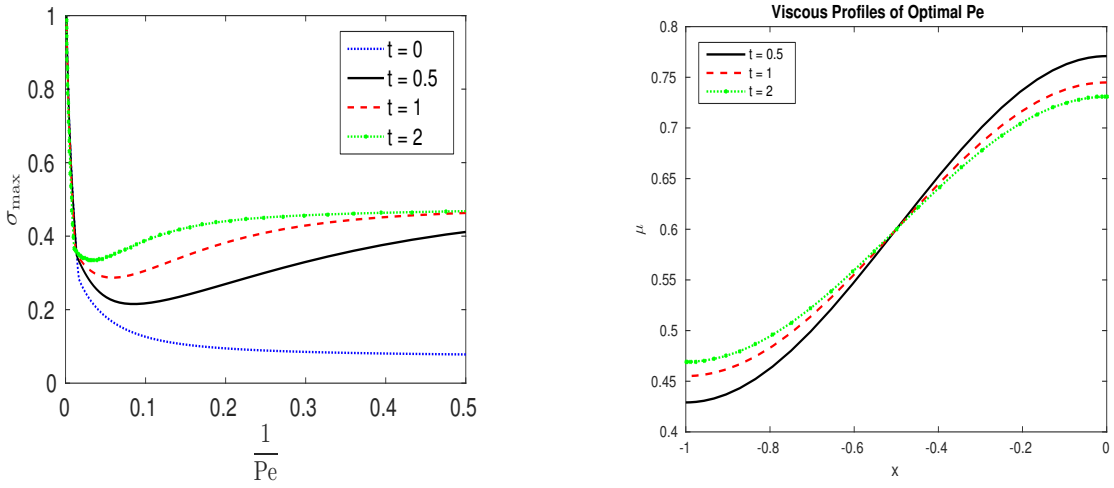

(a) (b)

Figure 13: The case of impermeable interfaces (with diffusion only): (a) A plot of σ_{max} versus $1/Pe$ at four different times. The initial viscous profile is linear with $\mu(-1) = 0.28$ and $\mu(0) = 0.92$. Notice that for $t > 0$, there is a particular value of Pe which minimizes σ_{max}. (b) Plots of the viscous profiles obtained at time $t = 0.25$ with $Pe = 6.1074$, at time $t = 0.5$ with $Pe = 10.2352$, and at time $t = 1$ with $Pe = 18.6946$. These values of Pe are the ones which minimize σ_{max} at their respective times in (a).

middle layer of fluid, this constant viscous profile is $\mu(x) = 0.6$. The constant viscosity case is well-studied (see [4, 5, 6, 9]), and the maximum growth rate using these parameters is $\sigma_{max} = 0.4103$. This limiting value is shown by the dotted line in Figure 14a.

4.3 Comparison of Permeable and Impermeable Interfaces

We now recap the numerical results of sections 4.1 and 4.2 with a comparison of the two types of interfaces. The main similarity between an impermeable and a permeable interface is that diffusion has a stabilizing effect and the effect is greater for steeper viscous profiles. This can be seen in Figures 4 and 11. However, there are some major differences between the two types of interfaces. In particular, the basic flow is time-independent for permeable interfaces but time-dependent for impermeable interfaces. Because of the time-dependent basic state for impermeable interfaces, increasing diffusion does not necessarily maximize stabilization at later times (see Figure 13a). This stands in contrast to the case of permeable interfaces in which increasing diffusion always enhances stability (see Figure 4).

In order to provide further comparison, we provide the dispersion relations for permeable and impermeable interfaces at four different Peclet numbers in Figure 15. In order to have a direct comparison, we consider the same initial viscous profile - a linear profile with $\mu(-1) = 0.36$ and $\mu(0) = 0.68$ - at all four Peclet numbers and for both types of interfaces. The viscous profile remains the same for the case of permeable interfaces but changes with time for the case of impermeable interfaces. Therefore, the growth rate is considered at three different times for impermeable interfaces. When $Pe = \infty$ (zero diffusion case), these two cases coincide and the dispersion relation is given by the top left figure. The dotted (red) line is the limiting value of σ as $k \to \infty$. Notice several features: (i) for each type of interface, higher values of diffusion are more stabilizing

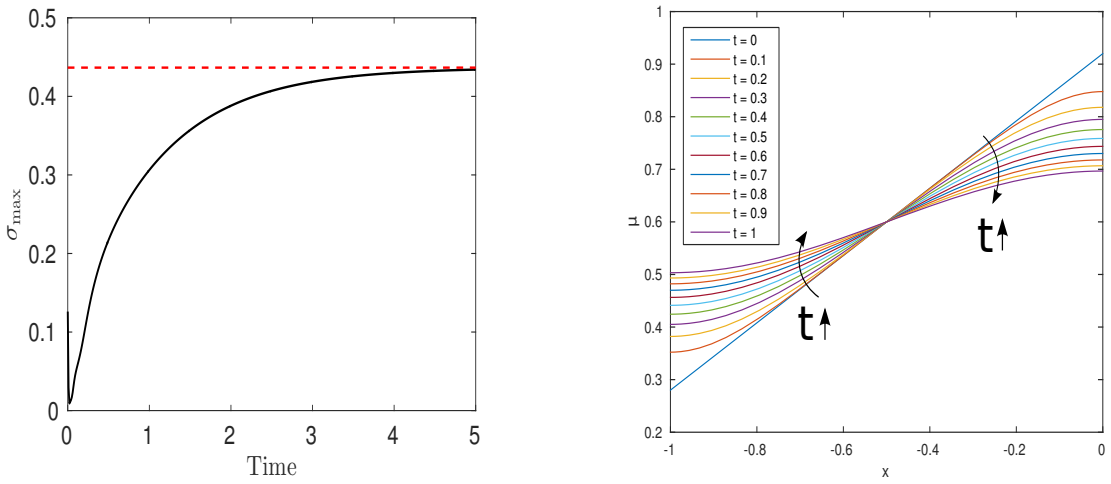

(a) (b)

Figure 14: The case of impermeable interfaces (with diffusion only): Plot (a) shows σ_{max} versus time. We use an initially linear viscous profile with $\mu(-1) = 0.28$ and $\mu(0) = 0.92$ and $Pe = 10$. The $t \to \infty$ limit is shown by the dotted line (red online). The evolution of the viscous profile from time $t = 0$ to time $t = 1$ is shown in plot (b).

globally as measured by $\sigma_{\max}$ and also locally or modally, i.e. for each wavenumber k. This is not surprising! (ii) The stabilizing effect of diffusion on the flow is greater with permeable interfaces than with impermeable interfaces. In particular, we see that the stabilizing effect is more pronounced with permeable interfaces for long waves. However, impermeable interfaces (see plots for $Pe = 100$ in Figure 15), can be more effective in suppressing the instability of short waves at later times because the initially linear viscous profile becomes less steep as time passes. Therefore, permeable interfaces are more effective for stronger diffusion or viscous profiles that are not very steep while impermeable interfaces are more effective for a steep profile and mild diffusion.

5 Dispersion

In order to include the effect of mechanical dispersion, we replace the dimensional equation (3) with

$$\frac{\partial c}{\partial t} + \mathbf{u} \cdot \nabla c = \nabla \cdot (\mathbf{D} \nabla c)\,, \tag{33}$$

where $\mathbf{D}$ is the dispersion tensor. Note that if $\mathbf{D}$ is equal to $D_0\mathbf{I}$, this reduces to the pure diffusion case, namely to equation (3). However, we now consider the case in which $\mathbf{D}$ has different components in the longitudinal and transverse directions, each of which depend on the velocity. These are denoted by $D_L(\mathbf{u})$ and $D_T(\mathbf{u})$, respectively. Then the tensor $\mathbf{D}$ can be written as [34]

$$\begin{aligned}\mathbf{D} &= \frac{1}{u^2+v^2}\begin{pmatrix} u & -v \\ v & u \end{pmatrix}\begin{pmatrix} D_L(\mathbf{u}) & 0 \\ 0 & D_T(\mathbf{u}) \end{pmatrix}\begin{pmatrix} u & v \\ -v & u \end{pmatrix} \\ &= D_T(\mathbf{u})\mathbf{I} + (D_L(\mathbf{u}) - D_T(\mathbf{u}))\frac{\mathbf{u}\mathbf{u}^{\mathbf{T}}}{||\mathbf{u}||^2},\end{aligned} \tag{34}$$

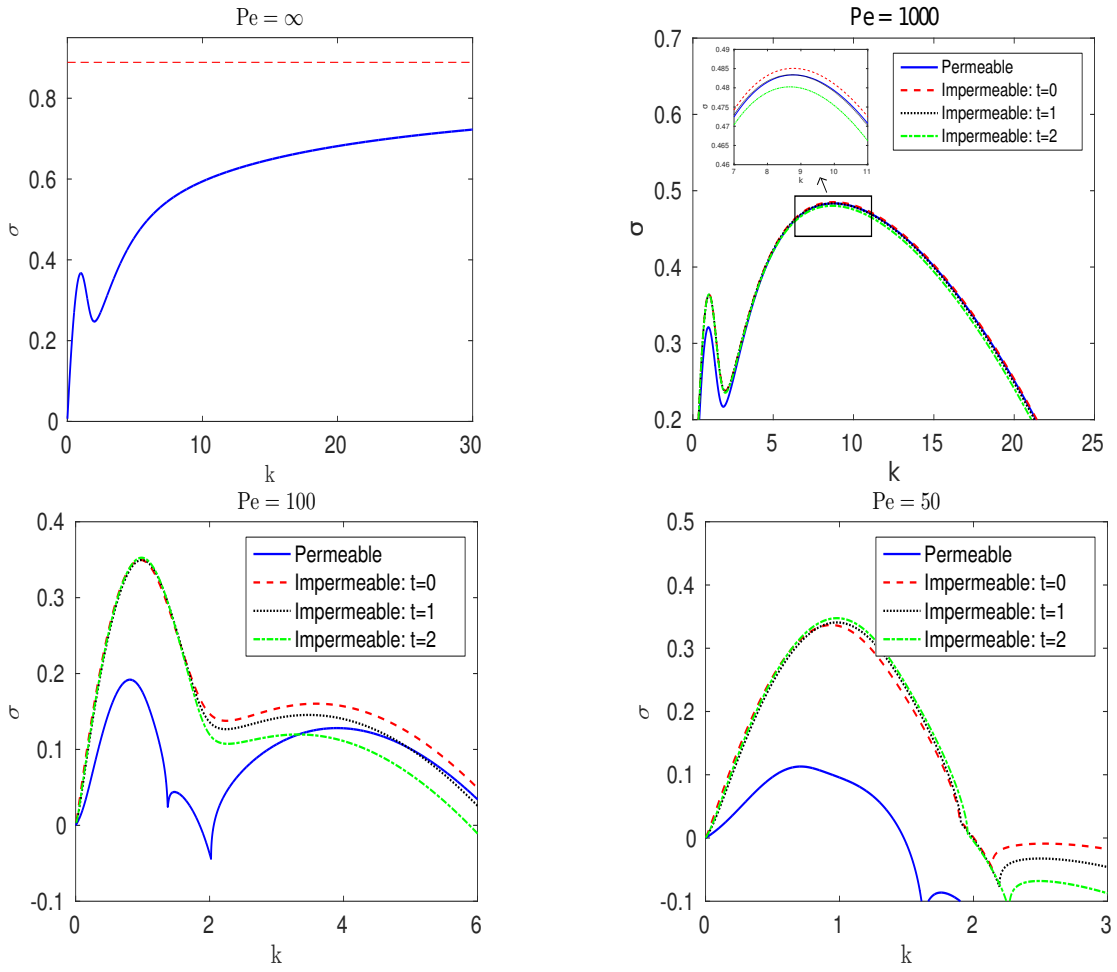

Figure 15: A comparison of the cases of permeable and impermeable interfaces (with diffusion only): The maximum value of the growth rate σ for each wavenumber k is plotted versus k for $\mu(-1) = 0.36$ and $\mu(0) = 0.68$ and for several different values of Pe. Recall $\mu_l = 0.2$ and $\mu_r = 1$. The dotted line in the top left plot represents the limit of σ as $k \to \infty$.

where $D_L(\mathbf{u})$ and $D_T(\mathbf{u})$ will be defined later (see equation (38)). In order to be consistent with the previous analysis which is done with no mechanical dispersion (see section 2), we consider a moving frame with velocity U in the positive x direction. We scale our equations using L as the characteristic length and U as the characteristic velocity. With a slight abuse of notation, below we use the same notations for dimensionless variables as for dimensional variables. The dimensionless equation in the moving frame is

$$\begin{aligned}\frac{\partial c}{\partial t} + \mathbf{u}\cdot\nabla c = &\frac{\partial}{\partial x}\left(\frac{D_T(\mathbf{u})}{UL}\frac{\partial c}{\partial x} + \left(\frac{D_L(\mathbf{u})}{UL} - \frac{D_T(\mathbf{u})}{UL}\right)\frac{1}{(u+1)^2+v^2}\left((u+1)^2\frac{\partial c}{\partial x} + (u+1)v\frac{\partial c}{\partial y}\right)\right)\\ &+ \frac{\partial}{\partial y}\left(\frac{D_T(\mathbf{u})}{UL}\frac{\partial c}{\partial y} + \left(\frac{D_L(\mathbf{u})}{UL} - \frac{D_T(\mathbf{u})}{UL}\right)\frac{1}{(u+1)^2+v^2}\left((u+1)v\frac{\partial c}{\partial x} + v^2\frac{\partial c}{\partial y}\right)\right). \qquad (35)\end{aligned}$$

The basic solution is for all the fluid to move in the positive x direction with velocity U. Therefore, in the moving frame, the velocity is $(u, v) = (0, 0)$. If we require that the basic concentration profile $c_0(x, t)$ be

independent of y, then from equation (35),

$$\frac{\partial c_0}{\partial t} = \frac{1}{Pe^*}\frac{\partial^2 c_o}{\partial x^2}, \tag{36}$$

where $Pe^* = (UL)/D_L(U,0)$. We perturb the basic solution $(u=0, v=0, c_0)$ by $(\widetilde{u}, \widetilde{v}, \widetilde{c})$. Plugging into equation (35) and linearizing with respect to the disturbances,

$$\frac{\partial \widetilde{c}}{\partial t} + \widetilde{u}\frac{\partial c_0}{\partial x} = \frac{1}{Pe^*}\left(\frac{\partial^2 \widetilde{c}}{\partial x^2} + \epsilon\frac{\partial^2 \widetilde{c}}{\partial y^2}\right) + \frac{\partial}{\partial x}\left\{\frac{\widetilde{u}}{L}\frac{\partial D_L(U,0)}{\partial u}\frac{\partial c_0}{\partial x} + \frac{\widetilde{v}}{L}\frac{\partial D_L(U,0)}{\partial v}\frac{\partial c_0}{\partial x}\right\} + \frac{1}{Pe^*}(1-\epsilon)\frac{\partial \widetilde{v}}{\partial y}\frac{\partial c_0}{\partial x}, \tag{37}$$

where $\epsilon = D_T(U,0)/D_L(U,0)$.

The above equation holds for any expression for D_L and D_T as long as they depend on the velocity. Therefore, it can be easily used with any of the available models for dispersion in the literature. Here, we use a common model for porous media, which is used in Ghesmat and Azaiez [18] and Ferreira et. al. [17]. The dispersion is given by

$$D_L(\mathbf{u}) = D_0 + a_L||\mathbf{u}||, \qquad D_T(\mathbf{u}) = D_0 + a_T||\mathbf{u}||. \tag{38}$$

Using (38) in (37),

$$\frac{\partial \widetilde{c}}{\partial t} + \widetilde{u}\frac{\partial c_0}{\partial x} = \frac{1}{Pe^*}\left(\frac{\partial^2 \widetilde{c}}{\partial x^2} + \epsilon\frac{\partial^2 \widetilde{c}}{\partial y^2}\right) + \frac{\partial}{\partial x}\left\{\gamma\frac{\partial c_0}{\partial x}\widetilde{u}\right\} + \frac{1}{Pe^*}(1-\epsilon)\frac{\partial \widetilde{v}}{\partial y}\frac{\partial c_0}{\partial x}, \tag{39}$$

where $\gamma = a_L/L$ is a measure of the strength of longitudinal dispersion. Using the ansatz (6) for the disturbances, equation (39) becomes

$$\frac{\partial h}{\partial t} = -\frac{\partial c_0}{\partial x}f + \frac{1}{Pe^*}\left(\frac{\partial^2 h}{\partial x^2} - \epsilon k^2 h\right) + \gamma\frac{\partial^2 c_0}{\partial x^2}f + \gamma\frac{\partial c_0}{\partial x}\frac{\partial f}{\partial x} - \frac{1}{Pe^*}(1-\epsilon)\frac{\partial c_0}{\partial x}\frac{\partial f}{\partial x}. \tag{40}$$

Therefore, with impermeable interfaces and dispersion, the eigenvalue problem which governs the growth of disturbances is (20) with $(20)_2$ replaced by

$$-\frac{\partial c_0}{\partial x}f + \frac{1}{Pe^*}\left(\frac{\partial^2 h}{\partial x^2} - \epsilon k^2 h\right) + \gamma\frac{\partial^2 c_0}{\partial x^2}f + \gamma\frac{\partial c_0}{\partial x}\frac{\partial f}{\partial x} - \frac{1}{Pe^*}(1-\epsilon)\frac{\partial c_0}{\partial x}\frac{\partial f}{\partial x} = \sigma h. \tag{41}$$

For the case of permeable interfaces, recall that the basic concentration profile is time independent and also linear with respect to x. Therefore, the eigenvalue problem for permeable interfaces is (23) with $(23)_2$ replaced by

$$-af + \frac{1}{Pe^*}\left(\frac{d^2 h}{dx^2} - \epsilon k^2 h\right) + a\gamma\frac{df}{dx} - \frac{a}{Pe^*}(1-\epsilon)\frac{df}{dx} = \sigma h. \tag{42}$$

5.0.1 Fourth Order Eigenvalue Problem

In order to get a single, fourth-order eigenvalue problem that accounts for dispersion, we use equation (24) in equation (41) for impermeable interfaces and in equation (42) for permeable interfaces. For impermeable interfaces,

$$\lambda\left\{\mu\frac{\partial^4 f}{\partial x^4} + 3\frac{\partial \mu}{\partial x}\frac{\partial^3 f}{\partial x^3} + \left(3\frac{\partial^2 \mu}{\partial x^2} - k^2(1+\epsilon)\mu\right)\frac{\partial^2 f}{\partial x^2} + \left(\frac{\partial^3 \mu}{\partial x^3} + (Pe^*\gamma - 3)k^2\frac{\partial \mu}{\partial x}\right)\frac{\partial f}{\partial x}\right.$$
$$\left. - k^2\left((1 - Pe^*\gamma)\frac{\partial^2 \mu}{\partial x^2} + Pe^*\frac{\partial \mu}{\partial x} - \epsilon k^2\mu\right)f\right\} = Pe^*\left(\mu\frac{\partial^2 f}{\partial x^2} + \frac{\partial \mu}{\partial x}\frac{\partial f}{\partial x} - k^2\mu f\right).$$

where $\gamma = a_L/L$ which is a measure of longitudinal mechanical dispersion. When $a_L = a_T$, (i.e. when $\epsilon = 1$), mechanical dispersion is isotropic.

For permeable interfaces, μ is a linear function of x so all higher order derivatives of μ are zero. Therefore, the fourth-order eigenvalue problem is

$$\lambda\left\{\mu\frac{\partial^4 f}{\partial x^4} + 3\frac{\partial\mu}{\partial x}\frac{\partial^3 f}{\partial x^3} - k^2(1+\epsilon)\mu\frac{\partial^2 f}{\partial x^2} + (Pe^*\,\gamma - 3)k^2\frac{\partial\mu}{\partial x}\frac{\partial f}{\partial x} - k^2\left(Pe^*\frac{\partial\mu}{\partial x} - \epsilon k^2\mu\right)f\right\}$$
$$= Pe^*\left(\mu\frac{\partial^2 f}{\partial x^2} + \frac{\partial\mu}{\partial x}\frac{\partial f}{\partial x} - k^2\mu f\right).$$

5.1 Numerical Results: Permeable Interfaces

We now consider some numerical results with the dispersion model introduced above. To understand some of these results, it is important to understand the relationship between Pe and Pe^*. Notice that equations (41) and (42) are similar to equations $(20)_2$ and $(23)_2$ but with Pe replaced by Pe^*. These two quantities are related in the following way.

$$Pe^* = \frac{Pe}{1 + Pe\,\gamma}, \qquad \text{and} \qquad Pe = \frac{Pe^*}{1 - Pe^*\,\gamma}.$$

The other two relevant parameters in this study are $\gamma = a_L/L$, which is the strength of longitudinal dispersion, and $\epsilon = D_T(U,0)/D_L(U,0)$, which is the ratio of transverse to longitudinal dispersion. When $\epsilon = 1$, the dispersion is isotropic and γ gives the strength of dispersion in both the longitudinal and transverse directions. If $\epsilon = 1$ and $\gamma = 0$, then there is no mechanical dispersion and the problem reduces to the one studied in section 4.

We start by considering the case of permeable interfaces. In Figure 16 we consider a linear viscous profile with $\mu(-1) = 0.36$ and $\mu(0) = 0.68$, and we plot σ_{max} versus $1/Pe$ to compare the cases of diffusion (with no mechanical dispersion) and dispersion. For the dispersion case, we use $\epsilon = 1$ (isotropic dispersion) and $\gamma = 0.01$ (which corresponds to very small mechanical dispersion). Notice that dispersion has a stabilizing effect and that this effect is especially strong when diffusion is mild. This is because when Pe is very large, $Pe^* \approx 1/\gamma$. Therefore, as $1/Pe \to 0$ and the effect of diffusion is lost, $1/Pe^* \to \gamma$ and the terms in the equation that are multiplied by $1/Pe^*$ still have an effect on stability.

Next, we consider the respective roles of transverse and longitudinal dispersion. In Figure 17 we again plot σ_{max} versus $1/Pe$ but this time for different amounts of transverse and longitudinal dispersion. In Figure (17a), the strength of the longitudinal dispersion pointwise is held constant at $\gamma = 0.01$ while the ratio of transverse to longitudinal dispersion, ϵ, is varied. When diffusion is mild (i.e. $1/Pe$ is small), the flow becomes more stable with increasing ϵ, i.e. with increasing transverse dispersion, but for strong diffusion, the trend is reversed. Recall from section 4 that short waves dominate the instability when diffusion is mild while long waves dominate the instability when diffusion is strong (see Figure 7). Increasing the strength of transverse dispersion has the effect of stabilizing short waves but has a destabilizing effect on long waves. Therefore, increasing the strength of transverse dispersion is stabilizing in the regime where short wave instability dominates (mild diffusion) and destabilizing when long wave instability dominates (strong diffusion). This point is illustrated by Figure 18. In Figure 18a, the dispersion relations are plotted for $Pe = 1000$ and for the same three values of ϵ that were considered in Figure 17a. When $Pe = 1000$, $\epsilon = 0.2$ is the most unstable because the shorter waves ($k \approx 6$) are most unstable. Figure 18b is the same

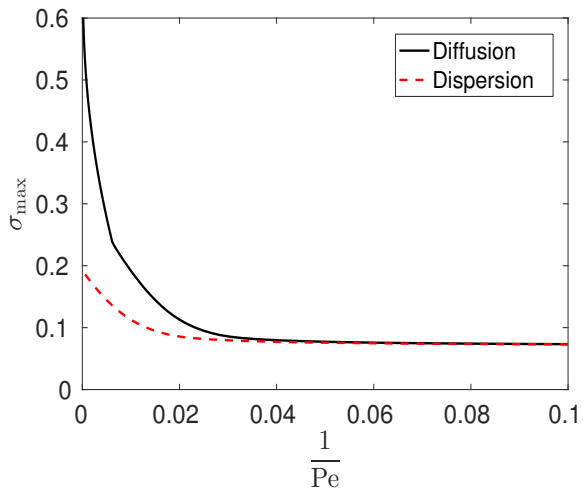

Figure 16: The case of permeable interfaces: A plot of σ_{max} versus $1/Pe$. The solid line is for the case of diffusion only (see section 4) and the dotted line includes dispersion. The viscous profile has $\mu(-1) = 0.36$ and $\mu(0) = 0.68$. The dispersion curve uses $\epsilon = 1$ (isotropic dispersion) and $\gamma = 0.01$. Recall that $\gamma = a_L/L$ and $\epsilon = D_T(U, 0)/D_L(U, 0)$.

plot but with $Pe = 50$. In this case, since longer waves are the most unstable ($k = 1$), $\epsilon = 5$ is the most unstable.

In Figure 17b, we consider the extreme cases of zero longitudinal dispersion but non-zero transverse dispersion ($a_L = 0, a_T/L = 0.01$) and zero transverse dispersion but non-zero longitudinal dispersion ($a_T = 0, a_L/L = 0.01$). In each case, γ and ϵ are chosen so that $a_T/L = 0.01$ or $a_L/L = 0.01$ as mentioned above. For most values of Pe within the range plotted, the presence of only longitudinal dispersion is more stabilizing than the presence of only transverse dispersion. The exception occurs only for very mild diffusion. This is because, as discussed above, longitudinal dispersion has a more stabilizing effect on long waves and transverse dispersion has a more stabilizing effect on short waves. For this particular choice of viscous profile, the long waves are most unstable except for very mild diffusion. Therefore, longitudinal dispersion is more stabilizing for all but this extreme case. This point about long and short waves can again be illustrated by looking at the dispersion relations for several different values of Pe. In Figure 19, these dispersion relations are plotted for $Pe = 1000$ and $Pe = 100$. In both cases, longitudinal dispersion (solid line) is more stabilizing for long waves and transverse dispersion (dotted line) is more stabilizing for short waves.

5.2 Numerical Results: Impermeable Interfaces

We now turn our attention to the effect of dispersion when the interfaces are impermeable. In order to provide an easy comparison with permeable interfaces, we consider the stability at time $t = 0$ with a linear viscous profile that has $\mu(-1) = 0.28$ and $\mu(0) = 0.92$. In Figure 20, we plot σ_{max} versus $1/Pe$ for the case where there is only diffusion and also when there is dispersion. We use the same amount of dispersion in both the longitudinal and transverse directions ($\epsilon = 1$ and $\gamma = 0.01$). For mild diffusion, the flow is more stable when there is dispersion. However for strong diffusion, dispersion has a destabilizing effect. As in the previous section, the difference can be attributed to short and long wave behavior. When diffusion is mild, the short wave behavior dominates the instability and when diffusion is strong, the long wave behavior

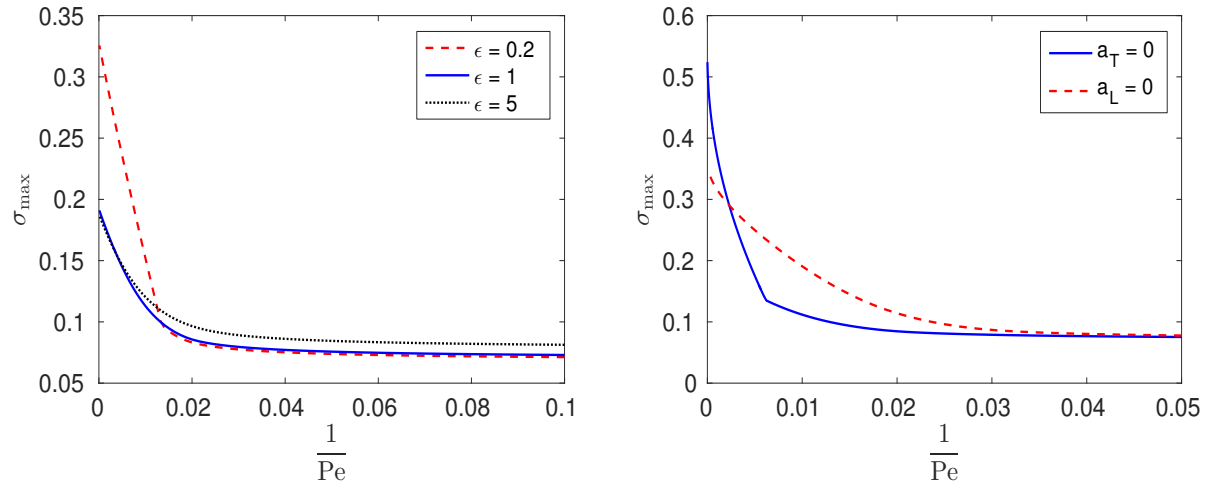

Figure 17: The case of permeable interfaces (with dispersion): Plot (a) shows σ_{max} versus $1/Pe$ for different values of ϵ when $\gamma = 0.01$. Plot (b) shows σ_{max} versus $1/Pe$ when $a_T = 0$ and $a_L/L = 0.01$ (solid line) and when $a_L = 0$ and $a_T/L = 0.01$ (dotted line). Both plots use a linear viscous profile with $\mu(-1) = 0.36$ and $\mu(0) = 0.68$. Recall that $\gamma = a_L/L$ and $\epsilon = D_T(U,0)/D_L(U,0)$.

dominates. Dispersion has the effect of stabilizing short waves and destabilizing long waves. This point is illustrated in Figure 21 in which we plot σ versus k for two different values of Pe. In both cases, the dispersion stabilizes short waves and destabilizes long waves. However, when $Pe = 100$, the maximum value of σ occurs for shorter waves and when $Pe = 50$ the maximum value of σ occurs for longer waves.

Finally, we consider the relative effects of longitudinal and transverse dispersion when the interfaces are impermeable. We consider a linear viscous profile with $\mu(-1) = 0.28$ and $\mu(0) = 0.92$ in Figure 22. In Figure 22a, the strength of the longitudinal dispersion is held constant at $\gamma = 0.01$ and the relative strength of the transverse dispersion is changed. Increasing transverse dispersion has a stabilizing effect. In Figure 22b, we consider the cases with only longitudinal dispersion and only transverse dispersion respectively. For flows with impermeable interfaces, having only transverse dispersion is more stabilizing.

5.3 Comparison of Dispersion for Permeable and Impermeable Interfaces

In sections 5.1 and 5.2, dispersion is found to have a very different effect for the two types of interfaces considered. For permeable interfaces, dispersion is stabilizing (see Figure 16) for all values of diffusion. This is also true for other viscous profiles which we do not show here because of space constraints. The stabilizing effect, as can be seen from this figure, is more dramatic for the case of mild diffusion but less so when diffusion is strong. For impermeable interfaces, dispersion can be stabilizing or destabilizing (see Figure 20) depending on the viscous profile and the strength of diffusion. The figure shows that dispersion is stabilizing for mild diffusion and destabilizing for strong diffusion.

Figure 21 shows a typical case in which dispersion is stabilizing for milder diffusion (corresponding to Pe=100) but destabilizing for stronger diffusion (corresponding to Pe=50). This behavior usually holds for other initial viscous profiles as well. Several observations can be made from Figure 21 about the stabilizing

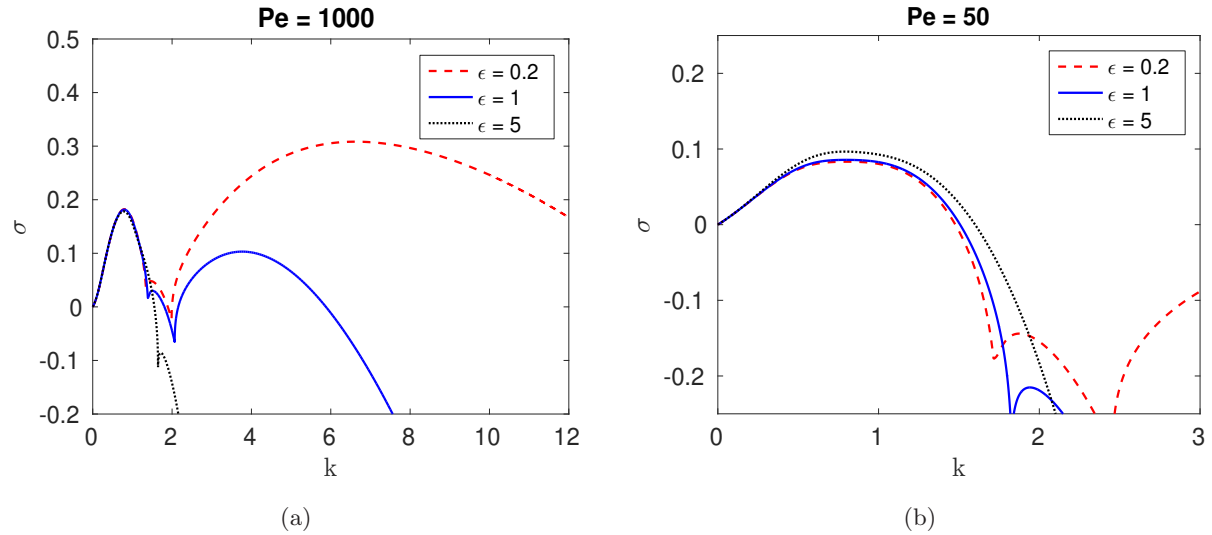

(a) (b)

Figure 18: The case of permeable interfaces (with dispersion): Plots of σ versus k for different values of ϵ when (a) $Pe = 1000$ and (b) $Pe = 50$. In both cases, $\gamma = 0.01$, $\mu(-1) = 0.36$ and $\mu(0) = 0.68$. Recall that $\gamma = a_L/L$ and $\epsilon = D_T(U,0)/D_L(U,0)$.

effect of dispersion with impermeable interfaces. Dispersion is stabilizing for short waves and destabilizing for long waves. The crossover from destabilizing to stabilizing in Fourier space takes place at a wave number which increases with the strength of diffusion (i.e. with decreasing Peclet number). In general, the short wave instability dominates when dispersion is stabilizing (see Figure 21a) and the long wave instability dominates when dispersion is destabilizing (see Figure 21b).

The two types of interfaces also behave differently with respect to longitudinal and transverse dispersion. For permeable interfaces, changing the strength of transverse dispersion while keeping longitudinal dispersion fixed can be stabilizing or destabilizing depending on the strength of diffusion (see Figure 17a). For impermeable interfaces, increasing the strength of transverse dispersion while keeping longitudinal dispersion fixed is always stabilizing (see Figure 22a). The two types of interfaces also exhibit different behavior in the extreme cases in which there is only longitudinal dispersion or only transverse dispersion. For permeable interfaces, the flow is more stable with only transverse dispersion for mild diffusion, but flows with only longitudinal dispersion are more stable for strong diffusion (see Figure 17b). For impermeable interfaces, flows with only transverse dispersion are always more stable than the ones with only longitudinal dispersion (see Figure 22b).

In order to have a more direct comparison of the stability of the flow with dispersion and each type of interface, the maximum value of σ versus k is plotted for permeable interfaces and for impermeable interfaces at three different times and for two different Peclet numbers (Figure 23). The viscous profile is initially linear with $\mu(-1) = 0.36$ and $\mu(0) = 0.68$. We use $\epsilon = 1$ (isotropic dispersion) and $\gamma = 0.01$. For both values of Pe, the flow becomes more stable as time increases for impermeable interfaces. This is due to the fact that the viscous profile is becoming less steep. However, flows with permeable interfaces are more stable than those with impermeable interfaces at all times. Recall from Figure 15 that in the absence of mechanical dispersion, permeable interfaces are more stable for strong diffusion. When dispersion is present, permeable interfaces gain an advantage for even milder diffusion (compare the top right of Figure 15 and Figure 23a

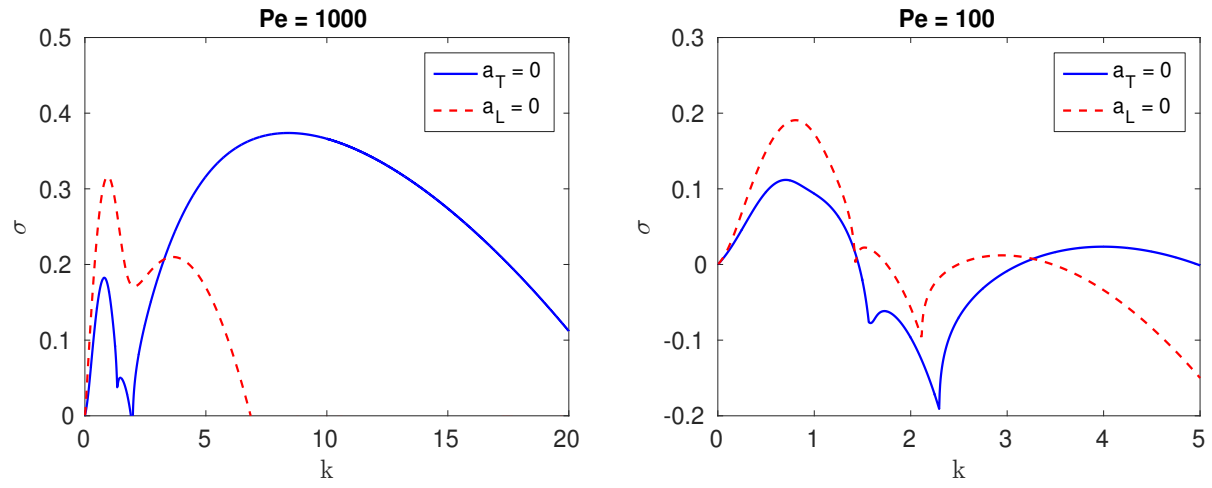

(a) (b)

Figure 19: The case of permeable interfaces (with dispersion): Plots of σ versus k when there is only longitudinal dispersion (solid line) and only transverse dispersion (dotted line). The Peclet numbers are (a) $Pe = 1000$ and (b) $Pe = 100$. In both cases $\mu(-1) = 0.36$ and $\mu(0) = 0.68$.

where $Pe = 1000$).

6 Summary

The work presented here is of fundamental interest to basic fluid mechanics of multi-layer flows and has direct relevance to many industrial processes including Enhanced Oil Recovery. In this work, the effect of diffusion and mechanical dispersion of polymer on the stability of multi-layer porous media flows for two different boundary conditions, corresponding to permeable and impermeable interfaces, are investigated. The linear stability equations are derived and the numerical results are presented and critically analyzed. In particular, for each of the two types of interfaces numerical data is used to determine the dependence of the absolute growth rate (flow instability) and of the dynamics of local (modal) instabilities on diffusion and mechanical dispersion. Some parameters, such as the Capillary number and the ratio of interfacial tensions, remain fixed for all simulations (recall $Ca = 10^{-3}$, $K^* = 10^{-4}$, $T_1/T_0 = 1$). Although these parameters have an effect on stability, the main goal of this study is to explore the effects of molecular diffusion and mechanical dispersion on flow stability. All of the qualitative trends and conclusions which are discussed appear to remain unchanged for different values of these parameters. These results have bearing on the design of "smart" interfaces that will be most stabilizing to flow and thus most desirable in cases where it matters such as in enhanced oil recovery.

We first look at the behavior of the growth rate, σ, when the concentration of polymer is held fixed at the interfaces (permeable interfaces). We obtain the following results: (i) diffusion is stabilizing, that is, it decreases the growth rate (see Figure 4); (ii) diffusion favors steeper viscous profiles (see also Figure 4); (iii) diffusion stabilizes short waves more than long waves (see Figure 7). For viscous profiles (see the top of Figure 4b) that are dominated by short wave instability in the absence of diffusion (see Figure 5c), there is a turning point (see Figure 4b). The short (long) wave instability dominates for diffusion that is milder

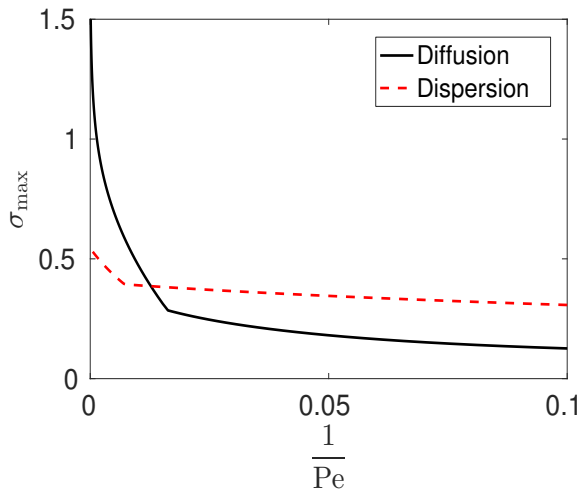

Figure 20: The case of impermeable interfaces: A plot of σ_{max} versus $1/Pe$. The solid line is for the case of pure diffusion (see section 4) and the dotted line includes dispersion. The viscous profile at $t = 0$ has $\mu(-1) = 0.28$ and $\mu(0) = 0.92$. The dispersion curve uses $\epsilon = 1$ (isotropic dispersion) and $\gamma = 0.01$. Recall that $\gamma = a_L/L$ and $\epsilon = D_T(U, 0)/D_L(U, 0)$.

(stronger) than that corresponding to the turning point; (iv) mild diffusion can lead to almost complete stability of the flow provided an optimal viscous profile is chosen (see Figure 10a). The optimal profile is typically more steep when diffusion is stronger (see Figure 10b).

We then proceed to numerically study the growth rate when there is no flux of polymer through the interfaces (impermeable interfaces). In contrast to the case of permeable interfaces, the viscous profile is time-dependent and tends toward a constant viscosity middle layer. Diffusion again has a stabilizing effect (see Figure 11a). Unless diffusion is very mild, increasing the strength of diffusion is not optimal for later times since it causes the viscous profile to approach its constant limit more quickly. For any given time $t > 0$, there is some optimal Peclet number that minimizes the maximum value of the growth rate (see Figure 13a).

Next, we provide a comparison of the stability for permeable and impermeable interfaces (see Figure 15). Increasing the strength of diffusion has a much more drastic stabilizing effect when the interfaces are permeable than when they are impermeable. However, if diffusion is mild and the viscous profile is steep, impermeable interfaces offer an advantage because the profile becomes less steep with time which reduces the instability due to the viscous gradient in the middle layer. Therefore, permeable interfaces provide greater stability when diffusion is relatively strong or when the viscous profile is not very steep, but impermeable interfaces are more stable for mild diffusion and steep viscous profiles.

We then investigate the effect of dispersion on the stability of the flow. For permeable interfaces, dispersion has a stabilizing effect (see Figure 16). However, this effect is dependent on the relative strength of longitudinal dispersion and transverse dispersion. Strong longitudinal (transverse) dispersion has the effect of stabilizing long (short) waves. Therefore, longitudinal (transverse) dispersion has a greater stabilizing effect for flows in which the long (short) wave instability dominates (see Figure 19)

When the interfaces are impermeable, dispersion is stabilizing for short waves and destabilizing for long waves (see Figure 21). Therefore, dispersion is not always stabilizing (see Figure 20). In contrast to permeable interfaces, transverse dispersion is more stabilizing than longitudinal dispersion for any value of

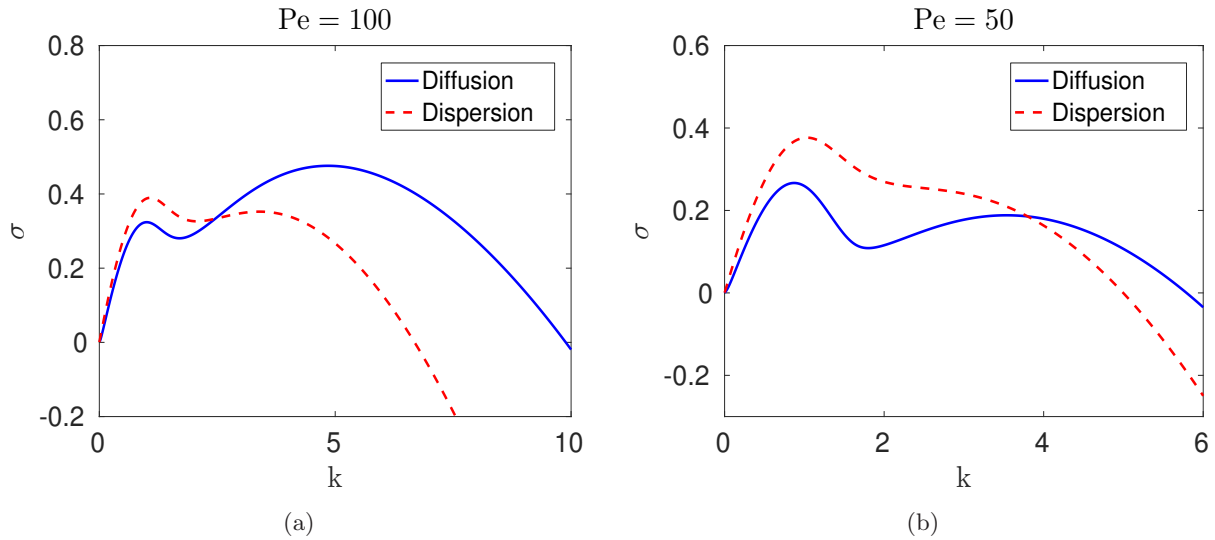

Figure 21: The case of impermeable interfaces: Plots of σ versus k with diffusion only (solid line) and with isotropic dispersion (dotted line). The Peclet numbers are (a) $Pe = 100$ and (b) $Pe = 50$. In both cases, the initial viscous profile is linear with $\mu(-1) = 0.28$ and $\mu(0) = 0.92$.

Pe (see Figure 22b).

We then compare the effect of dispersion for the two types of interfaces by considering isotropic dispersion for each with the same initial viscous profile. Permeable interfaces are found to be more stabilizing, in some cases significantly more stabilizing, than impermeable interfaces, even for cases of mild diffusion (see Figure 23).

7 Conclusion

There are several key findings of this paper which can be used to suppress the instability of three-layer porous media flows in applications like enhanced oil recovery. First, diffusion of polymer in the middle layer triggered by infinitesimal instabilities has a stabilizing effect on the flow for both permeable and impermeable interfaces. In general, this stabilizing effect is greater when the interfaces are permeable. In fact, when the interfaces are permeable the flow is almost completely stabilized by mild diffusion if the optimal viscous profile is chosen. This optimal viscous profile is steeper when diffusion is stronger. When the interfaces are impermeable the stabilization due to diffusion is not as much as in the permeable case. This is partly due to the fact that the viscous profile is time-dependent in this case and strong diffusion causes the viscous profile to more quickly approach its constant viscosity limit. Diffusion does not affect waves of all wavelengths the same. In general, diffusion stabilizes short waves more so than long waves. This leads to a "turning point" Peclet number (where short and long waves have the same growth rates) in the graphs of σ_{max} versus $1/Pe$ (see Figures 4 and 11). When diffusion is milder than that at the turning point, short waves are more unstable and when diffusion is stronger than the turning point, long waves are more unstable.

Mechanical dispersion also has an effect on the stability of the flow. When the interfaces are permeable, dispersion stabilizes the flow. This effect, coupled with the strong stabilizing effect of diffusion, leads to very nearly stable flows for permeable interfaces. When the interfaces are impermeable, dispersion is sometimes

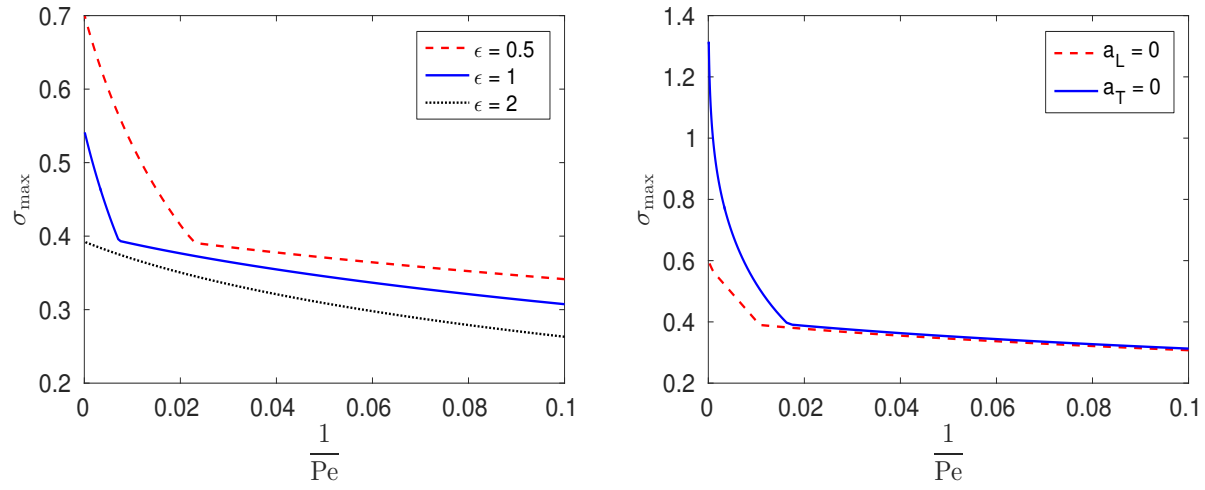

(a) (b)

Figure 22: The case of impermeable interfaces (with dispersion): Plot (a) shows σ_{max} versus $1/Pe$ for different values of ϵ when $\gamma = 0.01$. Plot (b) shows σ_{max} versus $1/Pe$ when $a_T = 0$ and $a_L/L = 0.01$ (solid line) and when $a_L = 0$ and $a_T/L = 0.01$ (dotted line). Recall that $\gamma = a_L/L$ and $\epsilon = D_T(U,0)/D_L(U,0)$.

stabilizing and sometimes destabilizing, which is a surprising result (see Figure 20). This depends on whether long or short waves are most unstable, which depends on both the strength of diffusion and the viscous profile.

For most realistic values of the parameters, flows with permeable interfaces are more stable than the corresponding flows with impermeable interfaces. If, in addition to designing the proper interfaces, the fluid in the middle layer has an optimal viscous profile and the strengths of diffusion and dispersion are not very mild, three layer porous media flows can be completely stabilized, even though less viscous fluids are driving more viscous fluids. Capillary number and the ratio of interfacial tensions have little effect on the key results.

Acknowledgments:

The work of P.D. was supported in part by the NPRP grant 08-777-1-141 through Qatar National Research Fund and by the U.S. National Science Foundation grant DMS-1522782. The authors would like to thank the reviewers for their constructive comments which significantly helped to improve the paper.

A Nomenclature

The following is a list of symbols used throughout this work along with their definitions followed by some mathematical relations between them.

Symbols:

μ - viscosity

μ_l - viscosity of the fluid in the leftmost layer

μ_r - viscosity of the fluid in the rightmost layer

$\mu(-1)$ - viscosity of the middle layer fluid at the trailing interface

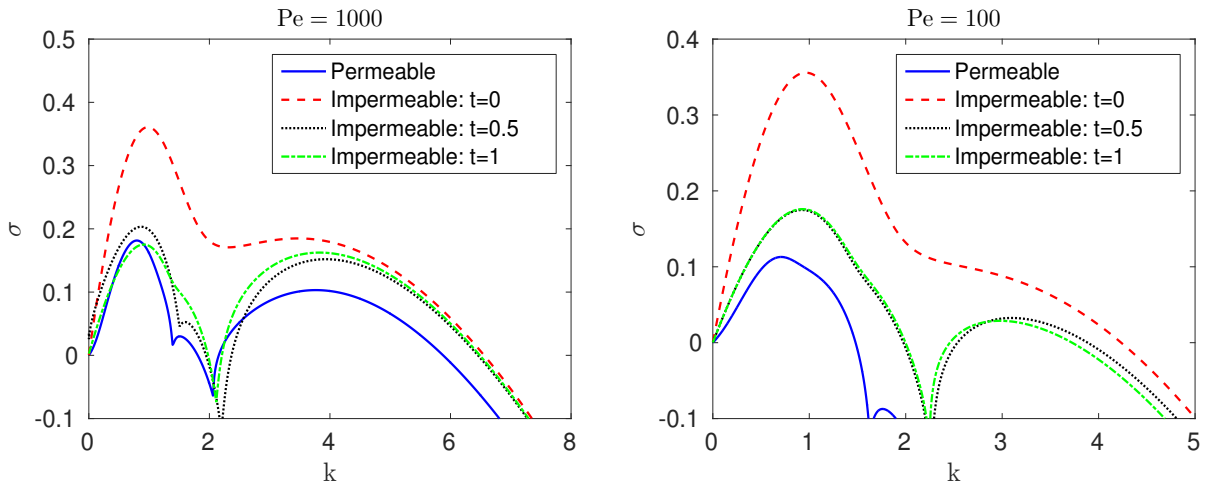

(a) (b)

Figure 23: A comparison of the cases of permeable and impermeable interfaces (with isotropic dispersion; $\epsilon = 1$ and $\gamma = 0.01$): The maximum value of the growth rate σ for each wavenumber k is plotted versus k for $\mu(-1) = 0.36$ and $\mu(0) = 0.68$ (at $t = 0$ for impermeable interfaces) and for several different values of Pe. Recall $\mu_l = 0.2$ and $\mu_r = 1$

$\mu(0)$ - viscosity of the middle layer fluid at the leading interface
T - interfacial tension
T_0 - interfacial tension at the leading interface
T_1 - interfacial tension at the trailing interface
$\mathbf{u}$ - velocity
p - pressure
K - permeability
c - concentration of polymer
D_0 - diffusion coefficient
K^* - dimensionless permeability
Pe - Peclet number
Ca - Capillary number
k - wavenumber of disturbance
σ - growth rate of disturbance
$\lambda = 1/\sigma$
D_L - longitudinal component of the dispersion tensor
D_T - transverse component of the dispersion tensor

Relations:
$K^* = \frac{K}{L^2}$
$Pe = \frac{UL}{D_0}$
$Ca = \frac{U\mu_r}{T_0}$

$Pe^* = \frac{UL}{D_L(U,0)}$
$D_L(\mathbf{u}) = D_0 + a_L||\mathbf{u}||$
$D_T(\mathbf{u}) = D_0 + a_T||\mathbf{u}||$
$\epsilon = \frac{D_T(U,0)}{D_L(U,0)}$
$\gamma = \frac{a_L}{L}$

B Numerical Method

Throughout the results sections above (Sections 4, 5.1, and 5.2), the eigenvalues of (29) and (32) and the corresponding equations with mechanical dispersion are computed numerically. The precise nature of the spectra of these operators is an open problem and worthy of future analytical study. In this section, we describe the pseudo-spectral Chebyshev method used to solve the eigenvalue problems, followed by a finite difference method used to verify the results and some verification results.

B.1 Pseudo-Spectral Chebyshev Method

In order to numerically compute the eigenvalues, we use a pseudo-spectral method. We first describe the method and then its application to our specific problem. For a more detailed treatment and proofs of convergence rates, see [3, 31].

Let $T_n(y)$ denote the n^{th} Chebyshev polynomial, which can be defined in terms of trigonometric functions as

$$T_n(y) = \cos(n \cos^{-1}(y)), \qquad y \in [-1, 1]. \tag{43}$$

The Chebyshev polynomials satisfy the orthogonality condition

$$\int_{-1}^{1} \frac{T_n(y)T_m(y)}{\sqrt{1-y^2}} dy = C_n \delta_{nm}, \tag{44}$$

where $C_0 = \pi$ and $C_n = \frac{\pi}{2}$ for $n \neq 0$. Additionally, the Chebyshev polynomials form a complete set with respect to the weight function $w(y) = \frac{1}{\sqrt{1-y^2}}$. Therefore, for any $f \in L^2_w([-1, 1])$, we may expand f as

$$f(y) = \sum_{n=0}^{\infty} a_n T_n(y), \qquad a_n = \frac{1}{\sqrt{C_n}} \int_{-1}^{1} \frac{f(y)T_n(y)}{\sqrt{1-y^2}} dy. \tag{45}$$

In order to use this expansion to solve our eigenvalue problem, we approximate the solution as the finite sum of the first $N + 1$ Chebyshev polynomials

$$f(y) \approx \sum_{n=0}^{N} a_n T_n(y). \tag{46}$$

In order to optimize the rate of convergence, we evaluate these at the extremal values of the Chebyshev polynomials (the Gauss-Chebyshev-Lobatto points), which are given by

$$y_j = \cos\left(\frac{j\pi}{N}\right), \qquad j = 0, ..., N. \tag{47}$$

Using these points, $T_n(y_j) = \cos\left(\frac{nj\pi}{N}\right)$. In order to solve an eigenvalue problem, we also need an expansion for the derivatives of f. We write the k^{th} derivative of f as

$$f^{(k)}(y) = \sum_{n=0}^{N} a_n T_n^{(k)}(y). \tag{48}$$

Using the change of variables $y = cos(\theta)$ and (43), we get $T_n(y) = \cos(n\theta)$. Therefore

$$T_n'(y) = \frac{n\sin(n\theta)}{\sin(\theta)}. \tag{49}$$

Using some trigonometric identities in (49), we arrive at the recurrence relation

$$T_n'(y) = 2nT_{n-1}(y) + \left(\frac{n}{n-2}\right) T_{n-2}'(y).$$

In general, for $k \geq 1$,the k^{th} derivative satisfies the recurrence relation

$$T_0^{(k)}(y) = 0, \qquad T_1^{(k)}(y) = T_0^{(k-1)}(y), \qquad T_n^{(k)}(y) = 2nT_{n-1}^{(k-1)}(y) + \left(\frac{n}{n-2}\right) T_{n-2}^{(k)}(y). \tag{50}$$

We may use this relation to build differentiation matrices in the following way. Let $\mathbf{a} = \{a_0, ..., a_N\}^T$ where the a_i's are the coefficients from (46). Let $\mathbf{D_0}$ be an $(N+1) \times (N+1)$ matrix such that the entry in row i and column j is given by

$$(\mathbf{D_0})_{i,j} = T_{j-1}(y_{i-1}). \tag{51}$$

Then $\mathbf{D_0 a} = \mathbf{f}$ where $\mathbf{f} = \{f(y_0), f(y_1), ..., f(y_N)\}^T$. We denote the k^{th} differentiation matrix by $\mathbf{D_k}$. Using (50), we can recursively build $\mathbf{D_k}$ from $\mathbf{D_{k-1}}$ using

$$(\mathbf{D_k})_{i,j} = T_{j-1}^{(k)}(y_{i-1}) = \begin{cases} 0, & j = 1, \\ (\mathbf{D_{k-1}})_{i,j-1}, & j = 2, \\ 2(j-1)(\mathbf{D_{k-1}})_{i,j-1} + \left(\frac{j-1}{j-3}\right)(\mathbf{D_k})_{i,j-2}, & 3 \leq j \leq N+1. \end{cases} \tag{52}$$

Then, for any $k \geq 0$, $\mathbf{D_k a} = \mathbf{f_k}$ where $\mathbf{f_k} = \{f^{(k)}(y_0), f^{(k)}(y_1), ..., f^{(k)}(y_N)\}^T$. For an explicit example of a MATLAB program that builds these matrices, see Schmid and Henningson [26, p. 491-492].

With these matrices, we can solve the eigenvalue problems (29) and (32) (and the equivalent problems with dispersion). Here, we only describe the method for (29) since it is easily adaptable to the other system of equations. Recall equation $(29)_1$:

$$\begin{aligned} &Pe\left(\mu f_{xx} + \mu_x f_x - k^2\mu f\right) \\ =&\lambda\left\{\mu f_{4x} + 3\mu_x f_{3x} + (3\mu_{xx} - 2k^2\mu)f_{xx} + (\mu_{3x} - 3k^2\mu_x)f_x - k^2(\mu_{xx} + Pe\mu_x - k^2\mu)f\right\}, \quad x \in (-1, 0) \end{aligned}$$

Note that the Gauss-Chebyshev-Lobatto points are in the interval $[-1, 1]$. We map these points to the interval $[-1, 0]$ using the affine map $x = \frac{1}{2}(y-1)$. Therefore, our collocation points are $x_i = \frac{1}{2}(y_i - 1)$. Additionally, since $\frac{d}{dx} = 2\frac{d}{dy}$, we let $\mathbf{D_k^x} = 2^k\mathbf{D_k}$. We require that equation $(29)_1$ hold at each collocation point, x_i, which gives a system of $N+1$ equations. Let $\mathbf{V^{(n)}}$ for $n = 0, 1, 2, 3$ be the matrices defined by

$$(\mathbf{V}^{(n)})_{i,j} = \begin{cases} \mu^{(n)}(x_{i-1}), & j = i, \\ 0, & \text{otherwise} \end{cases} \tag{53}$$

Then the i^{th} entry of the vector $\mathbf{V^{(n)}D_k^x a}$ is $\mu^{(n)}(x_{i-1})f^{(k)}(x_{i-1})$. Therefore, the condition that $(29)_1$ holds for each x_i is given by the matrix equation

$$\begin{aligned} &Pe\left(\mathbf{V^{(0)}D_2^x a}+\mathbf{V^{(1)}D_1^x a}-k^2\mathbf{V^{(0)}D_0^x a}\right)\\ =&\lambda\left(\mathbf{V^{(0)}D_4^x a}+3\mathbf{V^{(1)}D_3^x a}+(3\mathbf{V^{(2)}}-2k^2\mathbf{V^{(0)}})\mathbf{D_2^x a}+(\mathbf{V^{(3)}}-3k^2\mathbf{V^{(1)}})\mathbf{D_1^x a}-k^2(\mathbf{V^{(2)}}+Pe\mathbf{V^{(1)}}-k^2\mathbf{V^{(0)}})\mathbf{D_0^x a}\right). \end{aligned} \tag{54}$$

Let $\mathbf{A}=Pe\left(\mathbf{V^{(0)}D_2^x}+\mathbf{V^{(1)}D_1^x}-k^2\mathbf{V^{(0)}D_0^x}\right)$ and
$\mathbf{B}=\mathbf{V^{(0)}D_4^x}+3\mathbf{V^{(1)}D_3^x}+(3\mathbf{V^{(2)}}-2k^2\mathbf{V^{(0)}})\mathbf{D_2^x}+(\mathbf{V^{(3)}}-3k^2\mathbf{V^{(1)}})\mathbf{D_1^x}-k^2(\mathbf{V^{(2)}}+Pe\mathbf{V^{(1)}}-k^2\mathbf{V^{(0)}})\mathbf{D_0^x}$.
Then we have the generalized eigenvalue problem $\mathbf{Aa}=\lambda\mathbf{Ba}$. However, we must also enforce the boundary conditions. As in Schmid and Henningson [26, p. 489], we use the first, second, second to last, and last rows of our matrices to do it. The boundary conditions of (29) can be rewritten as

$$\begin{aligned} &\mu(0)f_x(0)+\mu_r\,kf(0)=\lambda E_0 f(0),\\ &\mu(0)f_{xxx}(0)+2\mu_x(0)f_{xx}(0)+\left(\mu_x x(0)-k^2\mu(0)\right)f_x(0)-k^2\mu_x(0)f(0)=-\lambda k^2\mu_{xx}(0)f(0),\\ &\mu(-1)f_{xxx}(-1)+2\mu_x(-1)f_{xx}(-1)+\left(\mu_x x(-1)-k^2\mu(-1)\right)f_x(-1)-k^2\mu_x(-1)f(-1)=-\lambda k^2\mu_{xx}(-1)f(-1),\\ &\mu(-1)f_x(-1)-\mu_l\,kf(-1)=-\lambda E_1 f(-1). \end{aligned}$$

Therefore, we use

$$\begin{aligned} &(\mathbf{A})_{1,j}=\mu(0)(\mathbf{D_1^x})_{1,j}+\mu_r k(\mathbf{D_0^x})_{1,j},\\ &(\mathbf{B})_{1,j}=E_0(\mathbf{D_0^x})_{1,j},\\ &(\mathbf{A})_{2,j}=\mu(0)(\mathbf{D_3^x})_{1,j}+2\mu_x(0)(\mathbf{D_2^x})_{1,j}+\left(\mu_{xx}(0)-k^2\mu(0)\right)(\mathbf{D_1^x})_{1,j}-k^2\mu_x(0)(\mathbf{D_0^x})_{1,j},\\ &(\mathbf{B})_{2,j}=-k^2\mu_{xx}(0)(\mathbf{D_0^x})_{1,j},\\ &(\mathbf{A})_{N,j}=\mu(-1)(\mathbf{D_3^x})_{N+1,j}+2\mu_x(-1)(\mathbf{D_2^x})_{N+1,j}+\left(\mu_{xx}(-1)-k^2\mu(-1)\right)(\mathbf{D_1^x})_{N+1,j}-k^2\mu_x(-1)(\mathbf{D_0^x})_{N+1,j},\\ &(\mathbf{B})_{N,j}=-k^2\mu_{xx}(-1)(\mathbf{D_0^x})_{N+1,j},\\ &(\mathbf{A})_{N+1,j}=\mu(-1)(\mathbf{D_1^x})_{N+1,j}-\mu_l k(\mathbf{D_0^x})_{N+1,j},\\ &(\mathbf{B})_{N+1,j}=-E_1(\mathbf{D_0^x})_{N+1,j}. \end{aligned}$$

We solve the generalized eigenvalue problem using MATLAB's "eig" command.

B.2 Finite Difference Method

In order to validate the pseudo-spectral Chebyshev method described above, we give a finite difference method which can be used to solve the eigenvalue problems. Here, we provide the method for the equation (32) (permeable interfaces without mechanical dispersion) and use it for a comparison with the pseudo-spectral method in Section B.3.

We can rewrite equation $(32)_1$ in terms of $\sigma=1/\lambda$ as

$$\begin{aligned} \frac{\mu}{Pe}\frac{d^4f}{dx^4}+\frac{3}{Pe}\frac{d\mu}{dx}\frac{d^3f}{dx^3}+\left(-\frac{2}{Pe}k^2\mu-\sigma\mu\right)\frac{d^2f}{dx^2}+\left(-\sigma\frac{d\mu}{dx}-\frac{3}{Pe}k^2\frac{d\mu}{dx}\right)\frac{df}{dx}\\ +\left(\left(\sigma+\frac{k^2}{Pe}\right)k^2\mu-k^2\frac{d\mu}{dx}\right)f(x)=0. \end{aligned} \tag{55}$$

The four boundary conditions for f in terms of σ are:

$$\left.\begin{array}{l}\mu(-1)\frac{df}{dx}(-1) = \left(\mu_l\, k - \frac{E_1}{\sigma}\right) f(-1),\\ -\mu(0)\frac{df}{dx}(0) = \left(\mu_r\, k - \frac{E_0}{\sigma}\right) f(0),\\ \mu(-1)\frac{d^2f}{dx^2}(-1) = \left\{k^2\mu(-1) - \frac{\frac{d\mu}{dx}}{\mu(-1)}\left(\mu_l\, k - \frac{E_1}{\sigma}\right) + \frac{k^2}{\sigma}\frac{d\mu}{dx}\right\} f(-1),\\ \mu(0)\frac{d^2f}{dx^2}(0) = \left\{k^2\mu(0) + \frac{\frac{d\mu}{dx}}{\mu(0)}\left(\mu_r\, k - \frac{E_0}{\sigma}\right) + \frac{k^2}{\sigma}\frac{d\mu}{dx}\right\} f(0).\end{array}\right\} \tag{56}$$

The stability problem is then defined by (55) and (56). This problem is discretized over the domain $(-1, 0)$ using $N+1$ uniformly spaced nodes with uniform step size $d = 1/N$. Therefore, the discretization points are given by $x_i = -1 + i/d$ for $i = 0, ..., N$. We use first order accurate approximation for the end point derivatives and second order approximation for the interior point derivatives, namely,

$$\left\{\begin{array}{l}\frac{df}{dx}(-1) = \frac{f(x_1)-f(x_0)}{d},\ \frac{df}{dx}(0) = \frac{f(x_N)-f(x_{N-1})}{d},\\ \frac{d^2f}{dx^2}(-1) = \frac{f(x_2)-2f(x_1)+f(x_0)}{d^2},\ \frac{d^2f}{dx^2}(0) = \frac{f(x_N)-2f(x_{N-1})+f(x_{N-2})}{d^2},\\ \frac{df}{dx}(x_i) = \frac{f(x_{i+1})-f(x_{i-1})}{2d}, \qquad i = 2, ..., N-2\\ \frac{d^2f}{dx^2}(x_i) = \frac{f(x_{i+1})-2f(x_i)+f(x_{i-1})}{d^2}, \qquad i = 2, ..., N-2\\ \frac{d^3f}{dx^3}(x_i) = \frac{f(x_{i+2})-2f(x_{i+1})+2f(x_{i-1})-f(x_{i-2})}{2d^3}, \qquad i = 2, ..., N-2\\ \frac{d^4f}{dx^4}(x_i) = \frac{f(x_{i+2})-4f(x_{i+1})+6f(x_i)-4f(x_{i-1})+f(x_{i-2})}{d^4} \qquad i = 2, ..., N-2.\end{array}\right.$$

The equation (55) is discretized using these formulas and after some algebraic manipulation yields

$$\begin{array}{l}\frac{1}{Pe}\left(\frac{\mu(x_i)}{d^4} - \frac{3}{2d^3}\frac{d\mu}{dx}\right) f(x_{i-2}) + \left\{-\frac{4\mu(x_i)}{d^4 Pe} + \frac{3}{d^3 Pe}\frac{d\mu}{dx} - \left(\sigma + \frac{2k^2}{Pe}\right)\frac{\mu(x_i)}{d^2} + \left(\sigma + \frac{3k^2}{Pe}\right)\frac{\frac{d\mu}{dx}}{2d}\right\} f(x_{i-1})\\ + \left\{\frac{6\mu(x_i)}{d^4 Pe} + 2\left(\sigma + \frac{2k^2}{Pe}\right)\frac{\mu(x_i)}{d^2} + (\sigma + \frac{k^2}{Pe})k^2\mu(x_i) - k^2\frac{d\mu}{dx}\right\} f(x_i)\\ + \left\{-\frac{4\mu(x_i)}{d^4 Pe} - \frac{3}{d^3 Pe}\frac{d\mu}{dx} - \left(\sigma + \frac{2k^2}{Pe}\right)\frac{\mu(x_i)}{d^2} - \left(\sigma + \frac{3k^2}{Pe}\right)\frac{\frac{d\mu}{dx}}{2d}\right\} f(x_{i+1}) + \frac{1}{Pe}\left(\frac{\mu(x_i)}{d^4} + \frac{3}{2d^3}\frac{d\mu}{dx}\right) f(x_{i+2}) = 0.\end{array}$$

Using the finite difference approximations in the boundary conditions given in equations (56) leads to

$$\left\{\begin{array}{l}\frac{f(x_1)-f(x_0)}{d} = \frac{1}{\mu(-1)}(\mu_l k - \frac{E_1}{\sigma})f(x_0)\\ \frac{f(x_N)-f(x_{N-1})}{d} = -\frac{1}{\mu(0)}(\mu_r k - \frac{E_0}{\sigma})f(x_N)\\ \frac{f(x_2)-2f(x_1)+f(x_0)}{d^2} = \frac{1}{\mu(-1)}\left\{k^2\mu(-1) - \frac{\frac{d\mu}{dx}}{\mu(-1)}\left(\mu_l\, k - \frac{E_1}{\sigma}\right) + \frac{k^2}{\sigma}\frac{d\mu}{dx}\right\} f(x_0)\\ \frac{f(x_N)-2f(x_{N-1})+f(x_{N-2})}{d^2} = \frac{1}{\mu(0)}\left\{k^2\mu(0) + \frac{\frac{d\mu}{dx}}{\mu(0)}\left(\mu_r\, k - \frac{E_0}{\sigma}\right) + \frac{k^2}{\sigma}\frac{d\mu}{dx}\right\} f(x_N)\end{array}\right.$$

which are rewritten as

$$\left\{\begin{array}{l}\left\{\left(\frac{\mu_l}{\mu(-1)}k + \frac{1}{d}\right)\sigma - \frac{E_1}{\mu(-1)}\right\} f(x_0) - \frac{\sigma}{d} f(x_1) = 0\\ -\frac{\sigma}{d} f(x_{N-1}) + \left\{\left(\frac{\mu_r}{\mu(0)}k + \frac{1}{d}\right)\sigma - \frac{E_0}{\mu(0)}\right\} f(x_N) = 0\\ \left\{\sigma\left(\frac{1}{d^2} - k^2 + \frac{\frac{d\mu}{dx}}{\mu(-1)}\frac{\mu_l k}{\mu(-1)}\right) - \frac{\mu_x}{\mu(-1)}\frac{E_1}{\mu(-1)} - k^2\frac{\frac{d\mu}{dx}}{\mu(-1)}\right\} f(x_0) - \frac{2\sigma}{d^2} f(x_1) + \frac{\sigma}{d^2} f(x_2) = 0\\ \frac{\sigma}{d^2} f(x_{N-2}) - \frac{2\sigma}{d^2} f(x_{N-1}) + \left\{\sigma\left(\frac{1}{d^2} - k^2 - \frac{\frac{d\mu}{dx}}{\mu(0)}\frac{\mu_r k}{\mu(0)}\right) + \frac{\mu_x}{\mu(0)}\frac{E_0}{\mu(0)} + k^2\frac{\frac{d\mu}{dx}}{\mu(0)}\right\} f(x_N) = 0\end{array}\right.$$

Using these finite difference approximations, the discrete analog of the problem defined by (55) and (56) is given by the following system of algebraic equations.

$$\mathbf{A}\mathbf{f} = 0, \tag{57}$$

where $\mathbf{f}$ is the vector with entries $f(x_0), f(x_1), f(x_2), ..., f(x_N)$ and $\mathbf{A}$ is a square matrix whose entries, now

denoted by $\mathbf{A}_{ij}$, $i,j = 1,2,...,(N+1)$, are given by

$$\mathbf{A}_{11} = \left(\frac{\mu_l}{\mu(-1)}k + \frac{1}{d}\right)\sigma - \frac{E_1}{\mu(-1)}, \quad \mathbf{A}_{12} = -\frac{\sigma}{d},$$
$$\mathbf{A}_{21} = \sigma\left(\frac{1}{d^2} - k^2 + \frac{\frac{d\mu}{dx}}{\mu(-1)}\frac{\mu_l k}{\mu(-1)}\right) - \frac{\mu_x}{\mu(-1)}\frac{E_1}{\mu(-1)} - k^2\frac{\frac{d\mu}{dx}}{\mu(-1)}, \quad \mathbf{A}_{22} = -\frac{2\sigma}{d^2}, \quad \mathbf{A}_{23} = \frac{\sigma}{d^2},$$
$$\mathbf{A}_{i,i-2} = \frac{1}{Pe}\left(\frac{\mu(x_i)}{d^4} - \frac{3}{2d^3}\frac{d\mu}{dx}\right),$$
$$\mathbf{A}_{i,i-1} = -\frac{4\mu(x_i)}{d^4 Pe} + \frac{3}{d^3 Pe}\frac{d\mu}{dx} - \left(\sigma + \frac{2k^2}{Pe}\right)\frac{\mu(x_i)}{d^2} + \left(\sigma + \frac{3k^2}{Pe}\right)\frac{\frac{d\mu}{dx}}{2d},$$
$$\mathbf{A}_{i,i} = \frac{6\mu(x_i)}{d^4 Pe} + 2\left(\sigma + \frac{2k^2}{Pe}\right)\frac{\mu(x_i)}{d^2} + (\sigma + \frac{k^2}{Pe})k^2\mu(x_i) - k^2\frac{d\mu}{dx},$$
$$\mathbf{A}_{i,i+1} = -\frac{4\mu(x_i)}{d^4 Pe} - \frac{3}{d^3 Pe}\frac{d\mu}{dx} - \left(\sigma + \frac{2k^2}{Pe}\right)\frac{\mu(x_i)}{d^2} - \left(\sigma + \frac{3k^2}{Pe}\right)\frac{\frac{d\mu}{dx}}{2d},$$
$$\mathbf{A}_{i,i+2} = \frac{1}{Pe}\left(\frac{\mu(x_i)}{d^4} + \frac{3}{2d^3}\frac{d\mu}{dx}\right), \quad \forall i \in [3, N-1]$$
$$\mathbf{A}_{N,N-1} = \frac{\sigma}{d^2}, \quad \mathbf{A}_{N,N} = -\frac{2\sigma}{d^2}, \quad \mathbf{A}_{N,N+1} = \sigma\left(\frac{1}{d^2} - k^2 - \frac{\frac{d\mu}{dx}}{\mu(0)}\frac{\mu_r k}{\mu(0)}\right) + \frac{\mu_x}{\mu(0)}\frac{E_0}{\mu(0)} + k^2\frac{\frac{d\mu}{dx}}{\mu(0)},$$
$$\mathbf{A}_{N+1,N} = -\frac{\sigma}{d}, \quad \mathbf{A}_{N+1,N+1} = \left(\frac{\mu_r}{\mu(0)}k + \frac{1}{d}\right)\sigma - \frac{E_0}{\mu(0)}.$$

B.3 Validation of the Numerical Method

Both the pseudo-spectral Chebyshev method and the finite difference method described above have been implemented in order to compare the results, and it was found that the methods agree. A typical plot of the maximum value of σ versus the wavenumber k is given in Figure 24 for each method for several different values of N, the number of grid points. These calculations are for permeable interfaces with the parameters values the same as those for Figure 7a ($Pe = 1000$, $Ca = 10^{-3}$, $K^* = 10^{-4}$, $T_1/T_0 = 1$, $\mu_l = 0.2$, $\mu(-1) = 0.36$, $\mu(0) = 0.68$, $\mu_r = 1$). There are two important points to note. First, both methods converge as the grid is refined and they converge to the same values. Second, the pseudo-spectral Chebyshev method converges much more quickly (the three curves corresponding to 10, 20, and 30 grid points are indistinguishable). The pseudo-spectral Chebyshev method has been used for the results section because of the fast convergence of the method and also because the run time is much shorter.

The method can be further validated by only accepting eigenvalues if they are found for more than one value of N [3]. In all cases considered in this paper, the eigenvalues that are agreed upon by different mesh sizes are real-valued. Of particular importance to this study is the fact that the value of σ with the largest real part is always real-valued and agreed upon by all possible mesh sizes.

References

[1] R. Aris, *On the dispersion of a solute in a fluid flowing through a tube*, Proceedings of the Royal Society of London Series A-Mathematical and Physical Sciences, 235 (1956), pp. 67–77.

[2] J. Bear, *Dynamics of fluids in porous media. Jacob Bear*, New York : Dover, 1988, 1988.

[3] J. Boyd, *Chebyshev and Fourier Spectral Methods*, Dover Publications, New York, 2001.

[4] P. Daripa, *Hydrodynamic stability of multi-layer Hele-Shaw flows*, J. Stat. Mech. Theory Exp., 12 (2008), p. 28.

[5] ——, *Studies on Stability in Three-Layer Hele-Shaw flows*, Phys. Fluids, 20 (2008).

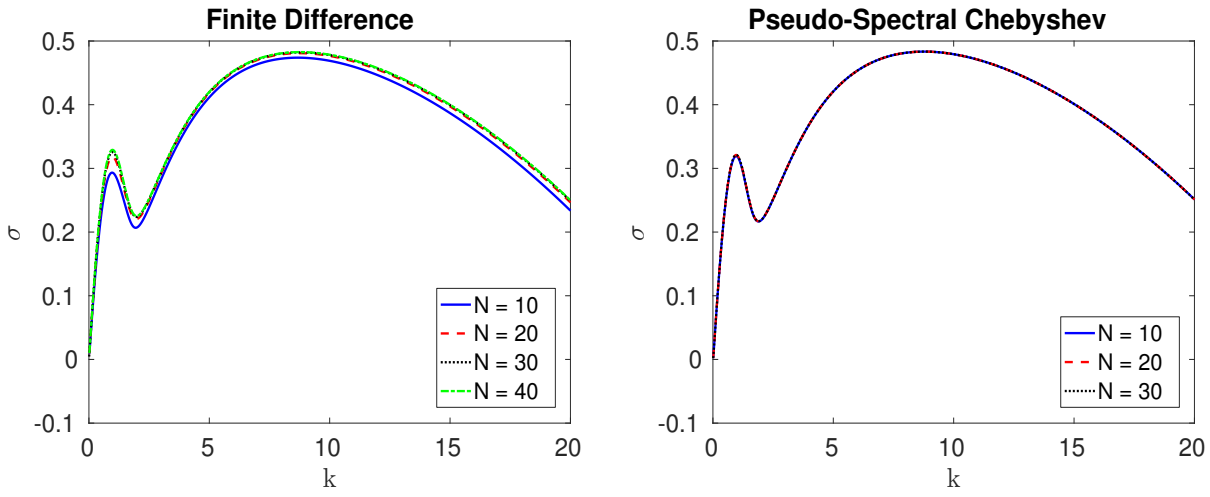

Figure 24: A comparison of the convergence of the two numerical methods: (a) finite difference and (b) pseudo-spectral Chebyshev. The maximum value of the growth rate σ for each wavenumber k is plotted versus k for permeable interfaces and diffusion only. The parameter values are the same as Figure 7a ($Pe = 1000$, $Ca = 10^{-3}$, $K^* = 10^{-4}$, $T_1/T_0 = 1$, $\mu_l = 0.2$, $\mu(-1) = 0.36$, $\mu(0) = 0.68$, $\mu_r = 1$).

[6] ——, *On estimates for short wave stability and long wave instability in three-layer Hele-Shaw flows*, Physica.A, 390 (2011), pp. 3069–3076.

[7] ——, *Some useful upper bounds for the selection of optimal profiles*, Physica.A, 391 (2012), pp. 4065–4069.

[8] P. Daripa and X. Ding, *A numerical study of instability control for the design of an optimal policy of enhanced oil recovery by tertiary dispalcement processes*, Transport in Porous Media, 93(3) (2012), pp. 673–703.

[9] ——, *Universal stability properties for multi-layer Hele-Shaw flows and application to instability control*, SIAM J. Appl. Math., 72 (2012), pp. 1667–1685.

[10] ——, *Selection principle of optimal profiles for immiscible multi-fluid Hele-Shaw flows and stabilization*, Transport in Porous Media, 96 (2013), pp. 353–367.

[11] P. Daripa, J. Glimm, B. Lindquist, and O. McBryan, *Polymer Floods: A Case Study of Nonlinear Wave Analysis And of Instability Control In Tertiary Oil Recovery*, SIAM J. Appl. Math., 48 (1988), pp. 353–373.

[12] P. Daripa and G. Pasa, *New bounds for stabilizing Hele-Shaw flows*, Appl. Math. Lett., 18 (2005), pp. 1293–1303.

[13] ——, *A simple derivation of an upper bound in the presence of a viscosity gradient in three-layer Hele-Shaw flows*, Journal of Statistical Mechanics, (2006), pp. 11 (doi:10.1088/1742–5468/2006/01/P01014).

[14] ——, *Stabilizing Effect of Diffusion in Enhanced Oil Recovery and Three-Layer Hele-Shaw Flows with Viscosity Gradient*, Tran. Porous Media, (2007), pp. 11–23.

[15] ——, *On Diffusive Slowdown in Three-Layer Hele-Shaw Flows*, Quart. Appl. Math., LXVIII (2010), pp. 591–606.

[16] P. G. Drazin and W. H. Reid, *Hydrodynamic Stability*, Cambridge Univ. Press., 1981.

[17] J. A. Ferreira, G. Pena, and G. Romanazzi, *Anomalous diffusion in porous media*, Applied Mathematical Modelling, 40 (2016), pp. 1850–1862.

[18] K. Ghesmat and J. Azaiez, *Viscous fingering instability in porous media: Effect of anisotropic velocity-dependent dispersion tensor*, Transport in Porous Media, 73 (2008), pp. 297–318.

[19] W. Littman, *Polymer Flooding: Developments in Petroleum Science*, Elsevier, Amsterdam, 1998.

[20] R. Maes, G. Rousseaux, B. Scheid, M. Mishra, P. Colinet, and A. De Wit, *Experimental study of dispersion and miscible viscous fingering of initially circular samples in hele-shaw cells*, Physics of Fluids, 22 (2010).

[21] R. Needham and P. Doe, *Polymer flooding review*, Journal of Petroleum Technology, 12 (1987), pp. 1503–1507.

[22] G. Pasa and O. Titaud, *A class of viscosity profiles for oil displacement in porous media or hele-shaw cell*, Transport in Porous Media, 58 (2005), pp. 269–286.

[23] T. PERKINS and O. JOHNSTON, *A review of diffusion and dispersion in porous media*, Society of Petroleum Engineers Journal, 3 (1963), pp. 70–84.

[24] P. Petitjeans, C. Chen, E. Meiburg, and T. Maxworthy, *Miscible quarter five-spot displacements in a hele-shaw cell and the role of flow-induced dispersion*, Physics of Fluids, 11 (1999), pp. 1705–1716.

[25] A. Riaz, C. Pankiewitz, and E. Meiburg, *Linear stability of radial displacements in porous media: Influence of velocity-induced dispersion and concentration-dependent diffusion*, Physics of Fluids, 16 (2004), pp. 3592–3598.

[26] P. Schmid and D. Henningson, *Stability and Transition in Shear Flows*, Springer, New York, 2001.

[27] C. Tan and G. Homsy, *Stability of miscible displacements in porous-media - rectilinear flow*, Phys. Fluids, 29 (1986), pp. 3549–3556.

[28] ——, *Stability of miscible displacements in porous-media - radial source flow*, Phys. Fluids, 30 (1987), pp. 1239–1245.

[29] G. Taylor, *Dispersion of soluble matter in solvent flowing slowly through a tube*, Proceedings of the Royal Society of London Series A-Mathematical and Physical Sciences, 219 (1953), pp. 186–203.

[30] ——, *Conditions under which dispersion of a solute in a stream of solvent can be used to measure molecular diffusion*, Proceedings of the Royal Society of London Series A-Mathematical and Physical Sciences, 225 (1954), pp. 473–477.

[31] L. Trefethen, *Spectral Methods in MATLAB*, Software, Environments, Tools, Society for Industrial and Applied Mathematics, Philadelphia, 2000.

[32] R. Wooding, *Instability of a viscous liquid of variable density in a vertical hele-shaw cell*, Journal of Fluid Mechanics, 7 (1960), pp. 501–515.

[33] Y. Yortsos and M. Zeybek, *Dispersion driven instability in miscible displacement in porous-media*, Physics of Fluids, 31 (1988), pp. 3511–3518.

[34] W. Zimmerman and G. Homsy, *Nonlinear viscous fingering in miscible displacement with anisotropic dispersion*, Physics of Fluids A, 3 (1991), pp. 1859–1872.